J Inorg Organomet Polym
DOI 10.1007/s10904-012-9694-8

REVIEW

Interactions of Metal Ions with DNA and Some Applications

Mohtashim Hassan Shamsi · Heinz-Bernhard Kraatz

Received: 13 February 2012 / Accepted: 3 May 2012

Abstract Nucleic acids play a critical role in life as we know it. It contains the necessary information required for the structure and function of a living organisms. Metal ions play a critical role in stabilizing conformations. In the well-known double helix structure of DNA, metal ions stabilize a particular conformation that ensures storage and propagation of genetic information. Metal ions, however, can interact with various sites on nucleic acids. Moreover, metal coordination can have a tremendous impact on the structure, conformation, stability and the electronic properties of the nucleic acids. The interactions are controlled by the relative affinity of metal ion coordination to the negatively charged phosphodiester backbone versus binding to other donor sites located in the nucleobases. The canonical Watson–Crick base pairs (A-T and G-C) as well as non-canonical base pairs (Hoogsteen and wobble) and mismatched pairs are often sites for metal ion interactions. In this review, an overview will be provided of the structure of different forms of nucleic acids (DNA and RNA) and the impact of different metal ions on their stability and structure. In addition, the recent applications of metal-DNA interactions in nanotechnology, biosensor and bioelectronics will also be discussed along with some therapeutic applications of metal complexes.

1 Introduction

Metal ions coordination to the nucleic acids (DNA and RNA) is critical for their structural properties and function. A number of factors play critical roles in controlling the particular effects on structure and function, including the nature of the metal ion, its charge and concentration, nucleic acid concentration, length and type of nucleic acid sequence, temperature, polarity of given solvent and buffer, and ionic strength. By and large, metal ions stabilize a particular nucleic acid structure and can lead to the denaturation of the native conformation, forming other structural motifs such as triple-strand formation, nucleic acid aggregation and condensation. In fact, all of these structural changes affect the in vivo nucleic acid functions [1]. A number of recent accounts highlight the growing interest in the interactions of metal ions and metal complexes with nucleic acids [2–5] in particular for therapeutic applications. In this review, we will provide an overview of the interactions between metal ions and double stranded DNA followed by some recent examples of applications emerging from DNA-metal interactions.

2 Structural Properties of Nucleic Acids

Deoxyribonucleic acid (DNA) is a biopolymer composed of nucleotide monomers. A nucleotide monomer is formed by a combination of three basic building blocks: a planar aromatic derivative of pyrimidine or purine base, a deoxyribose sugar and a phosphate group. There are two purine bases, adenine (A) and guanine (G) and two pyrimidine bases, thymine (T) and cytosine (C), involved in DNA structure (Fig. 1).

However, uracil (U), lacking the C5 methyl group, replaces thymine in mRNA. Inosine (I), a deaminated guanine analogue found in tRNA, can pair with C, U and A nucleobases in mRNA. Each nucleotide is joined with two other nucleotides in a polymeric chain through a phosphodiester bond in which a phosphate group links the 5′-end

M. H. Shamsi · H.-B. Kraatz (✉)
Department of Physical and Environmental Sciences, University of Toronto at Scarborough, 1265 Military Trail, Toronto, ON M1C 1A4, Canada
e-mail: bernie.kraatz@utoronto.ca

Published online: 08 June 2012

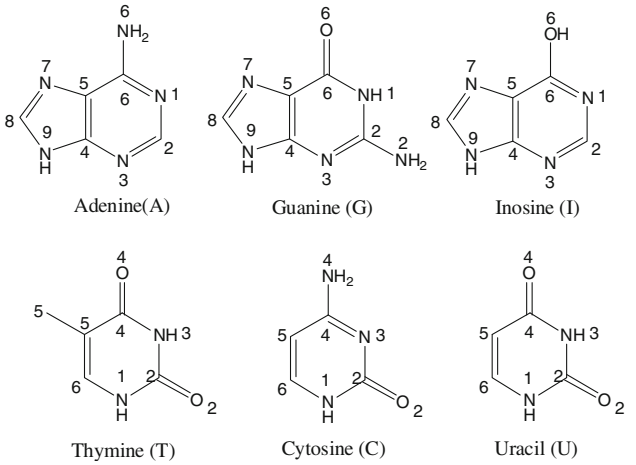

Fig. 1 Chemical structures of the nucleobases in DNA and RNA. Adenine (A), guanine (G), cytosine (C) and thymine (T) are found in deoxyribonucleic acid (DNA). Uracil (U), lacking C5 methyl group, replaces thymine (T) in mRNA while inosine (I), lacking 2-amino group of guanine, is found in tRNA and pairs with C, U and A in mRNA during translation in vivo. The *numbers* on atoms show their position around the ring

of sugar of one nucleotide to the 3′-end of the next nucleotide sugar. Thus, the polymerisation of nucleotides results in a long, single-stranded polyanionic chain, conventionally, in the 5′ → 3′ direction as a primary structure of the nucleic acid as shown in Fig. 2a. The sequence of these nucleobases in a DNA chain contains the precise information required to perform the specific functions inside the cell. DNA is mostly double-stranded (Fig. 2b) in its native form while paired regions occur intermittently throughout the structures adopted by RNA. The double-stranded helical structure of DNA is formed by the formation of hydrogen bonding between bases on opposite anti-parallel strands, often called "Watson–Crick base pairing", which involves purine–pyrimidine interstrand pairs [6]. This allows an 'A' to pair with a 'T' through two hydrogen bonds and a 'G' with a 'C' through three hydrogen bonds. In RNA, 'U' replaces the 'T' nucleobase in order to pair with 'A'. Any variation in this base pairing in DNA sequences is recognized as a mismatch which arises from insertion, deletion or translocation of a single or multiple nucleotides [7]. In fact, few other forms of base pairing also exist such as Hoogsteen and wobble base-pairs (Fig. 3), which are most common in RNA, however in DNA they are considered "base mismatches". The stability of the double-helical structure is further enhanced by π-π interactions between the stacked hydrophobic aromatic rings of adjacent bases on the polynucleotide chains [8].

3 Conformations of Double Stranded DNA

Double-stranded DNA is a highly polymorphic structure with three different conformations, A, B and Z as shown in Fig. 4a–c [9]. These conformational forms are not only affected by the primary sequence but also highly influenced by environmental factors such as hydration and ionic strength [10]. Under physiological conditions, the most common conformational form is B-DNA. It is a right-handed

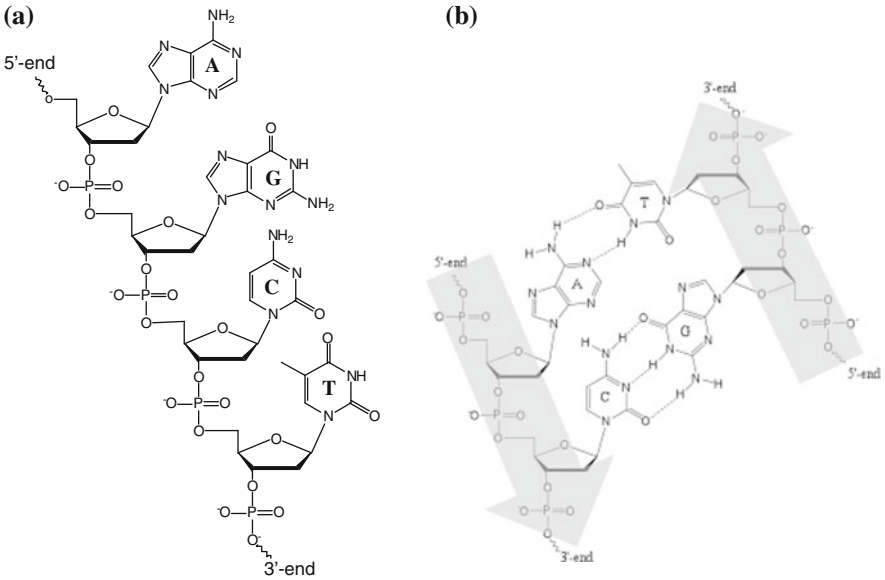

Fig. 2 Structural representation of **a** single stranded DNA where phosphodiester bonds link the 5′-end of sugar of one nucleotide to the 3′-end of the next nucleotide sugar, and **b** double stranded DNA where phosphate-sugar backbones running antiparallel (5′→3′/3′→5′) to each other and are bonded through two H-bonds between adenine (A) and thymine (T) nucleobases and three H-bonds between guanine (G) and cytosine (C) nucleobases, also known as Watson–Crick base-pairing. "Reprinted from Journal of Molecular Structure, 651–653, J. Anastassopoulou, Metal–DNA interactions, 19–26, Copyright (2003), with permission from Elsevier."

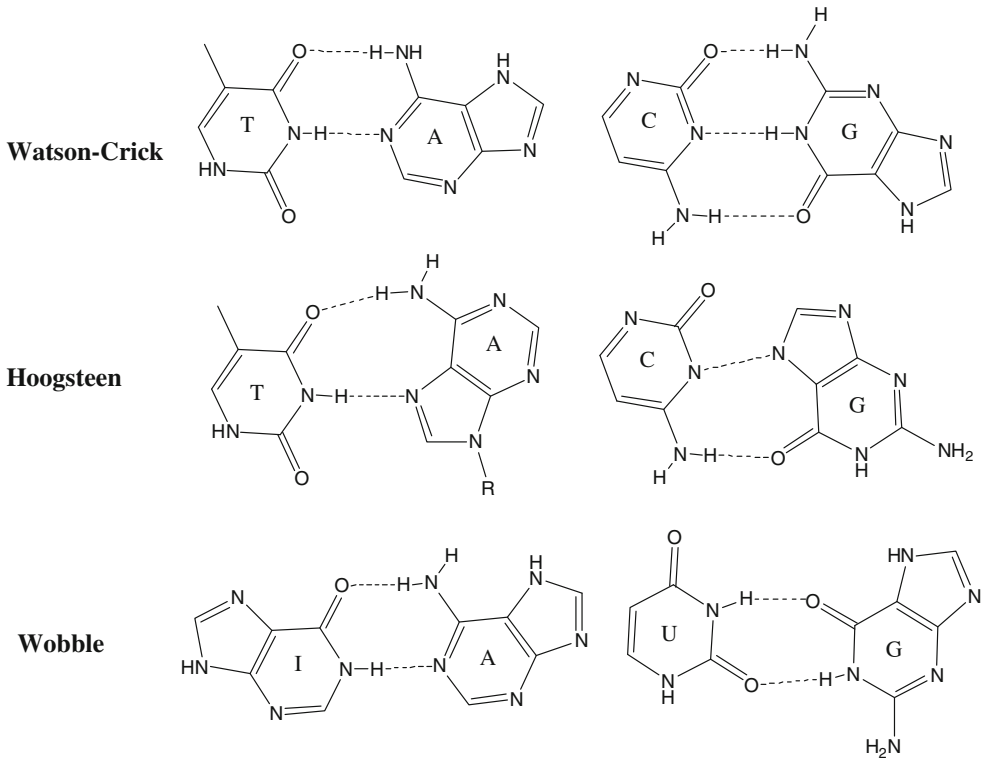

Fig. 3 Types of DNA base pairing. Watson–Crick model is the most common base pairing model in double stranded DNA where an A pairs with a T and a G pairs with a C through two and three hydrogen bonds respectively. Specifically, in A–T base pair the bonding atoms A_{N1} and A_{N6} pair with T_{N3} and T_{O4} respectively, while in G–C pair, G_{O6}, G_{N1} and G_{N2} engage in H-bonding with C_{N4}, C_{N3} and C_{O2} respectively. Hoogsteen base pairing is found in triple helices and i-motif quadruplexes. In a typical T–A Hoogsteen base pair, T_{N3} and T_{O4} pair with A_{N7} and A_{N6} respectively. In a C–G Hoogsteen base pair, C_{N3} and C_{N4} pair with G_{N7} and G_{O6} respectively. Wobble base pairing was proposed to explain the observed redundancy of mRNA codons that are recognized by the anticodon of tRNA. Inosine (I) in tRNA is involved in wobble base pairing with C, U and A in mRNA. In a typical I-A wobble pair, I_{N1} and I_{O6} pair with A_{N1} and A_{N6} respectively. In a U–G wobble pair, $U_{O2}$and U_{N3} pair with G_{N1} and G_{O6} respectively

helix with a diameter of approximately 20 Å, a pitch of 10.5 base pairs (bp) and a separation of 3.4 Å between two successive bases. The separation of sugar-phosphate backbone of the two anti-parallel strands due to base pair stacks and repulsion between anionic phosphate groups give rise to a pair of grooves that runs along the length of the duplex. These grooves facilitate base access [9, 11]. In canonical conformations, there are two kinds of grooves that exist, i.e., wide or major groove and narrow or minor groove. These grooves have specific dimensions. In *right-handed* B-DNA, major and minor grooves have similar depth of about 8 Å with different width of 11.6 and 6.0 Å respectively. The dimensions of these grooves are very sensitive to the base sequence of the duplex region of interest. For example, AT-rich sequences are known to adopt a narrower and more flexible minor groove than GC-rich regions. Groove width is defined as the perpendicular distance between phosphate groups on opposite strands, subtracting the 5.8 Å van der Waals diameter of a $–PO_4$ group, while groove depth is considered as differences in cylindrical polar radii between phosphorous and N2 guanine in minor groove or N6 adenine in major groove atoms [1].

In conditions of low hydration or high cationic strength, double stranded DNA can adopt the A-form, which is a *right-handed* compact double helical structure, with 11 bp per helical turn. In A-DNA, the bases are arranged away from the center of the helix resulting in a hollow core and wider structure [12]. The major groove of A-DNA has a width of 13 Å and very shallow depth of 2.2 Å. In contrast, the minor groove has slightly narrower width of 11.1 Å and also shallow depth 2.6 Å.

A third double helical conformation of ds-DNA also exists. Z-DNA forms a *left-handed* double helix, so named for its zig-zagging backbone [13]. This form has been observed at high ionic strengths, (≥2.5 M NaCl solutions) [14], or in modified form of DNA, such as methylated DNA [15]. Z and B forms are not mirror images since the B → Z transition requires inversion of bases to preserve the Watson–Crick pairing [16]. However, it has a flattened major groove having width of 8.8 Å and depth of 3.7 Å, while a deep (13.8 Å) and narrow (2.0 Å) minor groove, result in elongated and narrow structure relative to B-DNA. The parameters of the common conformers of double stranded DNA are summarized and compared in Table 1.

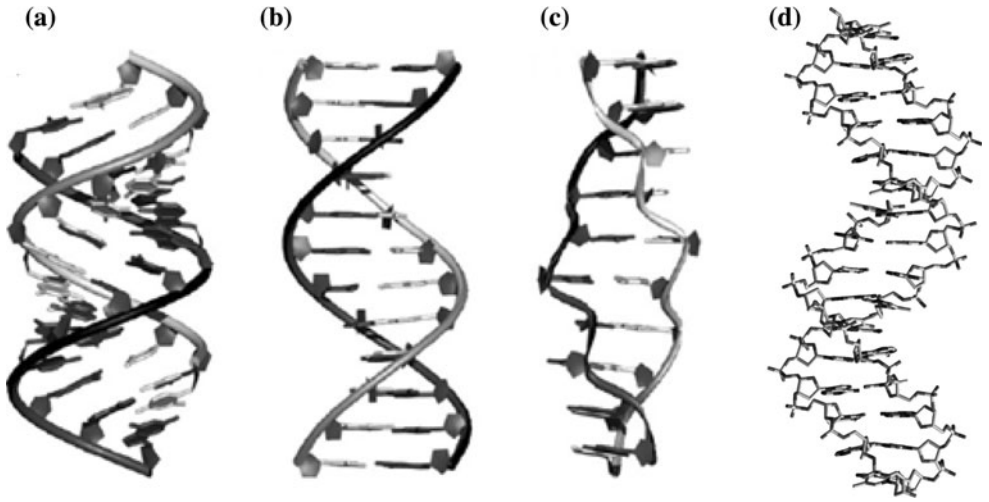

Fig. 4 Crystal structures of various conformations of double stranded DNA. **a** A-DNA is a right-handed helix with a pitch of 11 bp, a step height of 2.55 Å, a major groove width of 13 Å and a minor groove width of 11.1 Å. **b** B-DNA exists as a right-handed helix with a pitch of 10.5 bp, a step height of 3.4 Å, a major groove width of 11.6 Å and a minor groove width of 6.0 Å. **c** In contrast to the previous two forms, Z-DNA is a left-handed helix with a pitch of 11.6 bp, a step height of 3.7 Å, a major groove width of 8.8 Å and a minor groove width of 2.0 Å. Under physiological conditions, the B-DNA is the most stable structure for a random sequenced DNA molecule. Low hydration or high cationic strength conditions induce a B → A transition, while methylation of C5 cytosine can induce a conformational change B → Z. Moreover, metal complexes can induce the formation of a continuously stacked double helix with B → Z and Z → B transitions. "Reproduced from Müller [43] with permission of The Royal Society of Chemistry.", **d** Single crystal structure of Hoogsteen duplex of d(ATA^{Br}UAT) and d(ATATAT) with 10.6 base pairs per turn, minor groove width 9.3–11.1 Å. "Reproduced from Abrescia et al. [19]

Table 1 Parameters of common conformers of double stranded DNA

Properties	A-DNA	B-DNA	Z-DNA
Helical turn	Right-handed	Right-handed	Left-handed
Pitch (residues/turn)	11	10.5	11.6
Length/residue (Å)	2.55	3.4	3.7
Rotation/residue	32.7°	36.0°	−60°/2 bp
Inclination of bp towards axis	22.6°	2.8°	0.1°

Parameters adopted from [11]; S. Neidle, Nucleic Acid Structure and Recognition

While it was previously believed that an extremely high ionic strength is necessary for Z-DNA formation, it is now accepted that it is a transient form in vivo where it can be formed in the presence of cellular cations under physiological conditions [6]. Moreover, it has been shown that metal complexes can induce formation of a continuously stacked double helix with A → Z, B → Z and Z → B transitions [17, 18].

Abrescia et al. [19] demonstrated that an alternative to the classical B-DNA double helix is feasible under physiological conditions. Detailed X-ray crystallography confirmed a Hoogsteen double-helical structure for d(ATA^{Br}UAT) and d(ATATAT) sequences (Fig. 4d). The conformational parameters were found to be similar to those of duplex DNA in the B-form with 10.6 base pairs per turn, minor groove width 9.3–11.1 Å, where 'A' has two H-bond acceptor atoms (N1 and N3) in the major groove side and none in the minor groove, which shows that the Hoogsteen pairing influences the recognition sites of DNA.

In RNA, ribose possesses an additional hydroxyl group at the 2′-position which distinguishes RNA from DNA nucleotides (Fig. 5a). As the Watson–Crick base pairing between RNA nucleobases takes place, the ribose conformation changes from C2′-endo to C3′-endo (Fig. 5b) which converts the RNA double helix into A-form geometry (Fig. 5c). It is a right-handed helix which has a tilt of 18° with respect to the helix axis. Comparing to B-DNA, the A-RNA helix has a shorter pitch of 30 Å with 11 bp per turn and a diameter of 21 Å. A deep and narrow major groove and shallow minor grooves are formed due to the displacement of the base pairs in RNA. It was shown that the major groove of ds-RNA becomes more accessible for ligand binding at the end of the helices.

Thus, most of the binding sites for ligands in RNA structure are frequently formed by interruption in helical structure by bulges, loops, and non-Watson–Crick pairing. In high ionic strength media (∼6 M $NaClO_4$), left-handed Z-RNA is isostructural to Z-DNA. The A → Z transition in RNA is salt and alcohol concentration as well as temperature dependent. Modifications such as bromination of guanine and methylation of cytosine C5 in some cases may

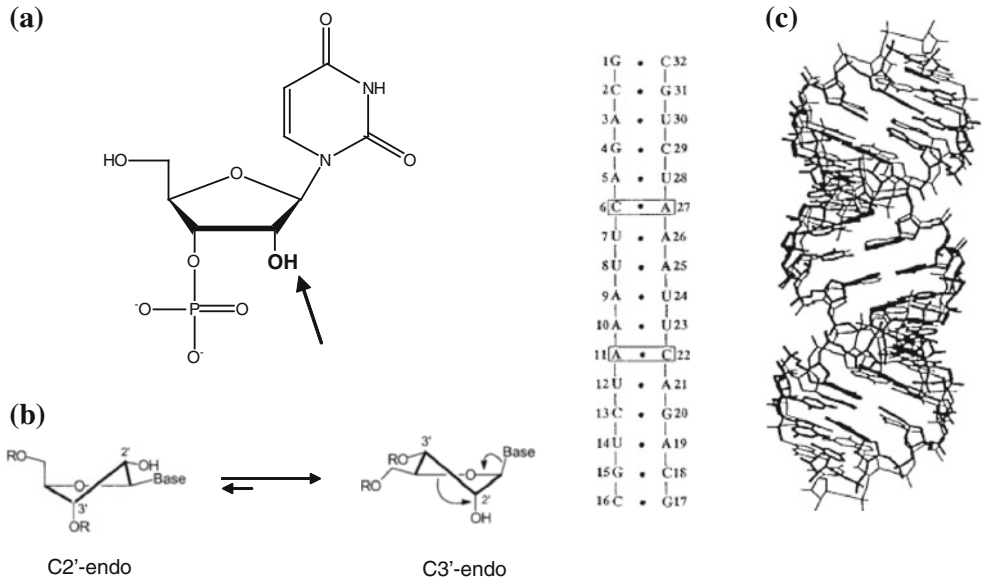

Fig. 5 Build up of RNA **a** chemical drawing of adenine ribonucleic acid, showing the 2′-OH which distinguishes RNA from DNA. **b** Conformation change of puckered sugar ring in RNA from C2′-endo to C3′-endo which helps in the formation of the A-RNA double helix. **c** Crystal structure of A-RNA of 16-mer r(GCAGA CUUAAAUCUGC)$_2$. The structure has two wobble C–A$^+$ base pairs at positions 6 and 11 (shown in *left*), however, an overall helical conformation is conserved (shown in *right*). "Reprinted from Pan et al. (1998), Structure of a 16-mer RNA duplex r(GCAGA CUUAAAUCUGC)$_2$ with wobble C·A$^+$ mismatches A-RNA, p. 977–984, with permission from Elsevier"

favour A → Z conversions. In contrast to B-DNA, no B-RNA has been reported. When A-RNA is destabilized, single strands are more stable than the B-form [20].

4 Mismatches in DNA Duplex

Mismatch base pairing occurs in both prokaryote and eukaryote cells during genetic recombination and/or replication and as a consequence of biosynthetic errors during nucleic acid synthesis. In this case, the nucleobases on opposite strands cannot form the typical 'Watson–Crick' base pairs. Examples of such mismatches within the DNA helix are transition mispairs in purine-pyrimidine pairs (G-T and A-C), as well as the transversion mismatches having purine–purine (G–G, A–A and G-A) and pyrimidine–pyrimidine (C–C, T–T and C-T) pairs; few examples are shown in Fig. 6a–d [21].

The wobble pairs are usually considered mispairs or mismatches in Watson–Crick base pairing. The X-ray analyses by Kennard [22] established that the G–T wobble base pair can be accommodated in the A [d(GGGGTC CC)], B [d(CGCGAATTTGCG)] or Z [d(TGCGCG)] double helices with minimal distortion of the overall conformation. The thermodynamic stability of the G–T wobble pair is comparable to that of the G–C and A–T base pairs. A study involving a double G–T mismatch in d(GGGG TCCC) [23] and d(GGGTGCCC) [24] duplexes showed the displacement of the bases into opposite grooves (T into deep groove and G into shallow groove) to accommodate wobble base pairs. Water molecules were able to H-bond to the exposed T_{O4} and G_{N2} atoms in the shallow and deep grooves. This interaction stabilizes the overall structure. The displacement of the bases into the grooves causes a change in the twist angle by ∼10° per wobble pair, explaining the unusually high (44°) and low (25°) twist at the central TpG and GpT steps of the above octamers respectively. A–C and G–T base pairings appear to be similar (see Fig. 6e) [25]. However, a solvent molecule links the bases on the major groove side to enhance stability, but not on minor groove side. In this case, adenine is either protonated or in rare tautomeric form.

5 Effect of Mismatch on DNA Structure and Stability

Roongta et al. [26] studied a series of dodecamers of the type d(CG*T*GAATTCGCG) varying five different types of single nucleotide mismatches at position 3 (G–T, G–G, G–A, A–C, and G–U). ^{31}P NMR study showed a significant signal shift of the phosphate group adjacent to the mismatch in position 2. Perturbations at other sites were significantly more complex. While effects due to a G–T or G–U base pair mismatch were largely localized to the base pairs adjacent to the mismatch site, A–C, G–A, and G–G mismatches create major distortions in the backbone structure, which allows the detection of the distortion several base pairs further from the

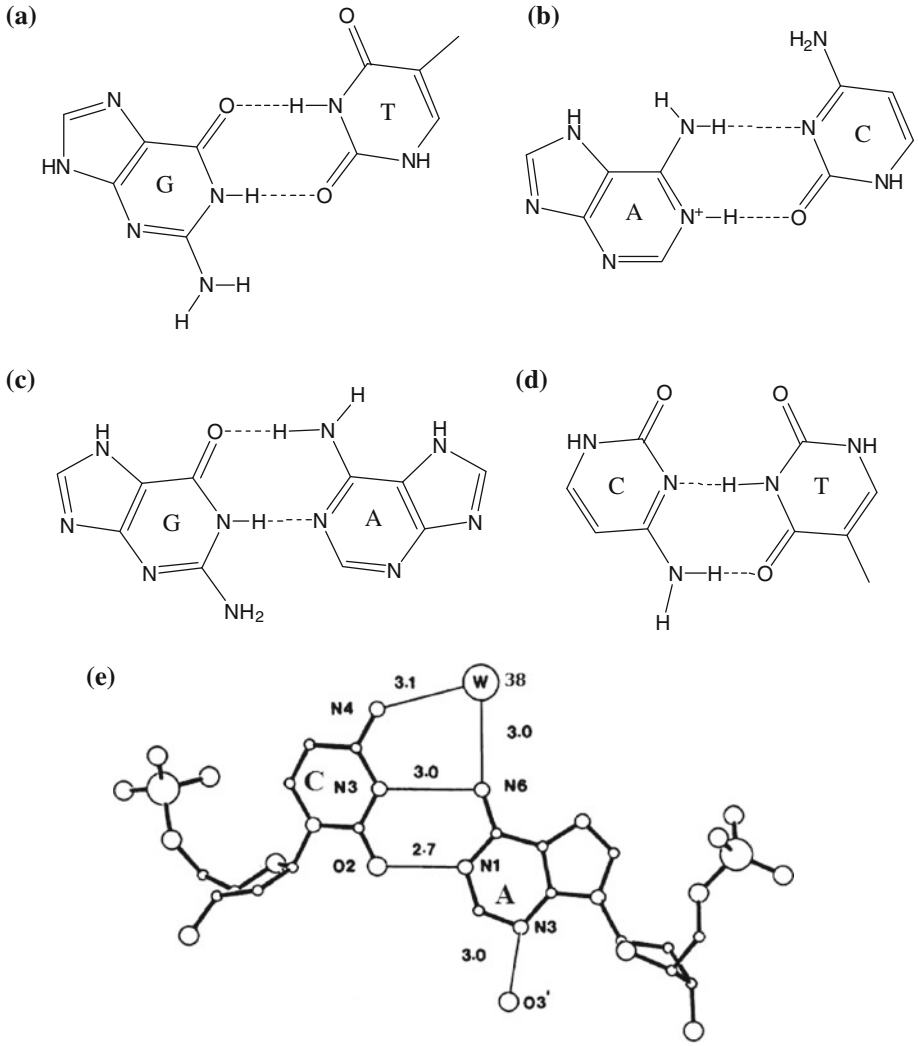

Fig. 6 Drawings of the DNA mismatches **a** G–T, **b** A–C, **c** G–A, and **d** C–T. **e** Crystal structure of a C–A mismatch with associated water molecule. Atoms involved in H-bonds are labelled and distances given in Å. "Reproduced from Hunter [25], by permission of Oxford University Press."

mismatch position. ^{31}P NMR shift values are summarized in Table 2. In contrast, Patel et al. [27] demonstrated that the local geometry for a G–A mismatch base pair is not distorted much beyond the mismatch itself. A Raman study on a G–T wobble base pair at position 2 in d(CGCG*C*G) sequence confirmed a maximum change in the Raman intensity of the O–P–O linkage around the mismatch in B-DNA, while there is no measureable change for Z-DNA [28]. Due to the presence of mismatch, changes in the deoxyribose phosphate backbone may take place at one or all of the angles from α–ζ: P^{α}–$O5'^{\beta}$–$C5'^{\gamma}$–$C4'^{\delta}$–$C3'^{\varepsilon}$–$O3'^{\zeta}$–P as shown in Fig. 7. Changes in the P–O torsional angles (α and ζ) and C–O torsional angles (β and ε) influence ^{31}P chemical shifts significantly. Local helical parameters can be changed due to the structural perturbations in the duplex, such as helical twist and/or base pair roll. Gorenstein et al. [29] showed that the changes in these local parameters generally alter the length of the deoxyribose phosphate backbone. The greatest variation in backbone torsional angles is observed for ζ(P–O3′) followed by ε(C3′–O3′).

The presence of a mismatch destabilizes a duplex relative by 1.7–10.0 kcal/mol depending upon position and type of mismatch as well as concentration of Na^+ ions [30], consequently lowering the melting temperature T_m [31]. The thermodynamic destabilization of a mismatched base pair duplex relative to the perfectly matched duplex comes from perturbations in nearest neighbour interactions and hydrogen bonding. The mismatch stability series G–T> G–G>G–A>C–T>A–A = T–T>A–C = C–C was reported by Aboul-Ela et al. [32] and there are some variability in such reports depending on the sequence environment and the nearest-neighbour of the mismatch [33]. The effect of sequence environment, in a 18-mer DNA, was also supported by the fact that the flipping of the mismatch from T–G by G–T or G–A by A–G caused the difference in free energy by 0.7–0.9 kcal/mol at room temperature [34]. X-ray crystallographic data [35] and NMR [36] study of DNA with G–T mismatches exhibit local deformation in sugar-phosphate backbone structure and some changes in the π-stacking. Nevertheless, the global helicity

Table 2 ^{31}P NMR chemical shifts of the five mismatches at position 3 in 12-mer d-(CG*T*GAATTCGCG)

Position	G–T[a]		G–G[b]		G–A[b]		G–U[b]		A–C[b]	
	Seq.	^{31}P Shifts	Seq.	^{31}P Shifts	Seq.	^{31}P Shifts	Seq.	^{31}P Shifts	Seq.	^{31}P Shifts
1	C	−4.078	C	−4.198	C	−4.140	C	−4.177	C	−4.211
2	G	−4.670	G	−4.198	G	−3.493	G	−4.713	G	−3.783
3	*T*	−3.897	*G*	−4.198	*A*	−4.292	*U*	−3.909	*C*	−4.003
4	G	−4.371	G	−4.345	G	−4.140	G	−4.420	G	−4.159
5	A	−4.408	A	−4.462	A	−4.571	A	−4.494	A	−4.561
6	A	−4.523	A	−4.548	A	−4.246	A	−4.691	A	−4.665
7	T	−4.463	T	−4.375	T	−4.005	T	−4.518	T	−4.509
8	T	−4.247	T	−4.044	T	−4.444	T	−4.323	T	−4.656
9	C	−4.047	C	−4.486	C	−4.069	C	−4.079	C	−4.146
10	G	−4.386	G	−4.132	G	−4.521	G	−4.420	*A*	−4.327
11	C	−4.154	C	−4.132	C	−4.150	C	−4.177	C	−4.003

^{31}P NMR chemical shifts reference is TMP (trimethyl phosphate) at room temperature

Reproduced from Roongta et al. [26]

[a] The ^{31}P resonances of the GT 12-mer were assigned by site-specifically labelling each phosphate with ^{17}O Gorenstein et al. [29]

[b] The ^{31}P resonances of all the other mismatches were assigned by using 31P/1H HECTOR (PAC) 2D experiment

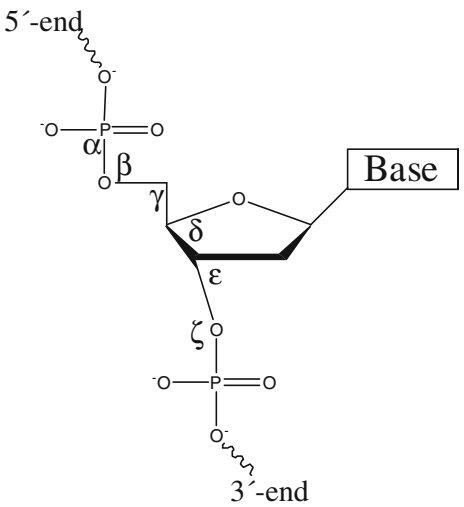

Fig. 7 Drawing depicting the torsional angles α–ζ along the sugar-phosphate backbone from 5′-end to 3′-end P^{α}-$O5'^{\beta}$-$C5'^{\gamma}$-$C4'^{\delta}$-$C3'^{\varepsilon}$-$O3'^{\zeta}$-P in a nucleotide

(conformation) is conserved. Again, the mismatch stability is sequence dependent, and mismatch next to the G–C pairs are more stable than the A–T base pairs.

Single nucleotide mismatches are the most frequent genetic variation within the human genome. Although, under normal conditions, the DNA repair machinery and polymerase proof-reading mechanisms correct the gene alteration. However, these repair systems may fail and result in a large number of mismatches [37]. While a number of diseases are related to single base pair mismatches within the ds-DNA [38], by and large incorporation of such mismatches pushes the evolutionary envelope. In the case of mismatches leading to human diseases, their identification is critical, and would allow monitoring of genetic diseases, viral infections and even certain cancers [39]. It is critical to appreciate that mismatches are dynamic structures, i.e. they can interact with small molecules and metal ions, which can be useful for their detection.

6 Overview of Interaction between Metal Ions and DNA

Metal cations have significant roles in the structure and physiological functions in a living cell. For instance, Na^+/K^+ pump in transport process across the cell membrane, Zn^{2+} and Co^{2+} work as co-factors in enzymatic processes, Fe^{2+}/Fe^{3+} in oxygen transport process etc. Moreover, divalent cations are also required for the replication, transcription and translation of the genetic code [40]. Metal ions are also involved in the stabilization of the DNA structure by coordination to the phosphodiester backbone of DNA [9]. Specifically, in the absence of any cations, the native double-helical B-conformation of DNA cannot be formed and, thus DNA is unable to perform its functions [41]. However, small, mobile, multivalent cations can bring about structural change in DNA, such as bending. In fact, Rouzina and Bloomfield demonstrated that a multivalent cation binds at the access of major groove of the

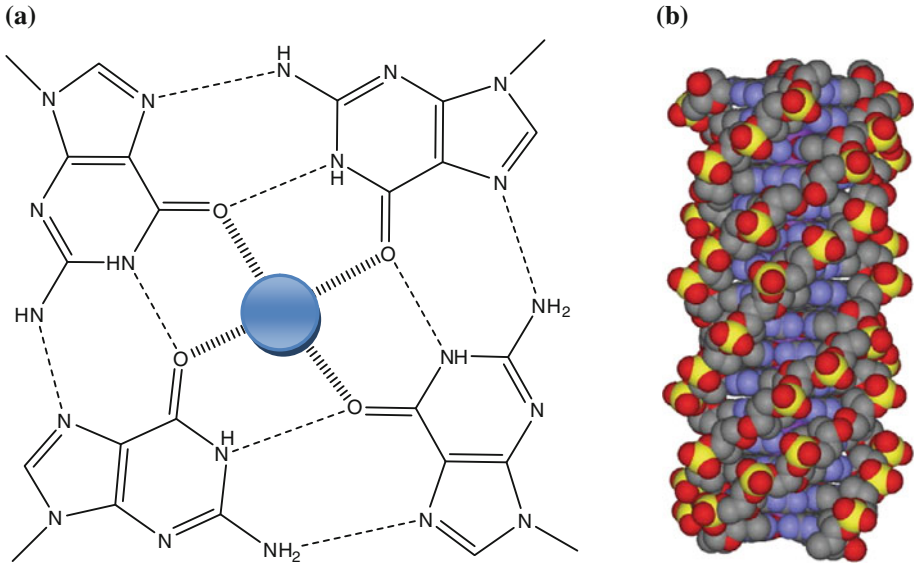

Fig. 8 **a** The arrangement of guanine bases in the G-quartet, shown together with a centrally placed metal ion. Hydrogen bonds are shown as *dotted lines*. **b** Space-filled model of G-quadruplex DNA, which is poly(dG) four-fold, right-handed helix. "Reproduced from Burge et al. (2006), Quadruplex DNA: sequence, topology and structure, Nucleic Acids Research, 2006, 34, 19, 540, by permission of Oxford University Press"

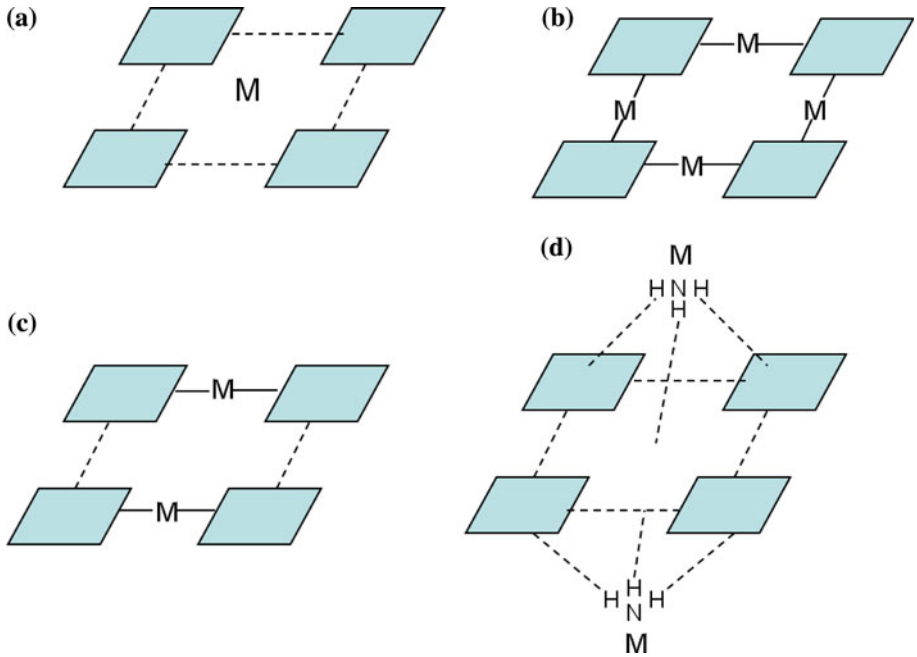

Fig. 9 Schematic showing different binding patterns between metal ions (M) and the nucleobases (*blue tiles*) that form nucleobase quartets [7]: **a** metal ion 'M' in center of nucleobase quartet with H bonds (*solid lines*) between the bases, **b** cyclic purine quartet with four metals cross-linking the purines, **c** association of metallated base pairs via H-bonding, and **d** $[M]NH_3$ groups above and below the quartet with H-bonding between the four bases and NH_3

B-DNA, between the two phosphate strands. Consequently, the phosphates on both strands are strongly attracted to the groove-bound cation. This causes groove closure and finally DNA bending towards the cationic ligand [42].

Base pairing of nucleobases within the strand (e.g. RNA) or between two different stands (e.g. DNA) in conjunction with metal coordination (usually Mg^{2+}) leads to distinct structural patterns and structure of higher order, for instance DNA triple helices, G-quadruplex, and helical junctions [43]. In fact, Davis proposed as early as 1962 that guanine-rich sequences of DNA can assume very unusual structures, in which the guanines could form planar H-bonded arrangements called guanine quartets (Fig. 8) [44]. These arrangements are stabilized by metal ion coordination. G-quartets (also known as quadruplexes, tetraplexes or G4-structures) play an important biological role in telomeres, which protect the ends of chromosomes and can be an effective drug target. Different binding patterns between the metal ions that form nucleobase quartets are depicted in Fig. 9, earlier discussed by Lippert [45].

7 Types of Interaction between Metal Ions and DNA

There are generally two types of interaction between the DNA and metal ions, (a) ligand-mediated interactions and (b) direct metal ion bonding with DNA. Ligand-mediated interactions occur via H-bond, π–π interactions between a

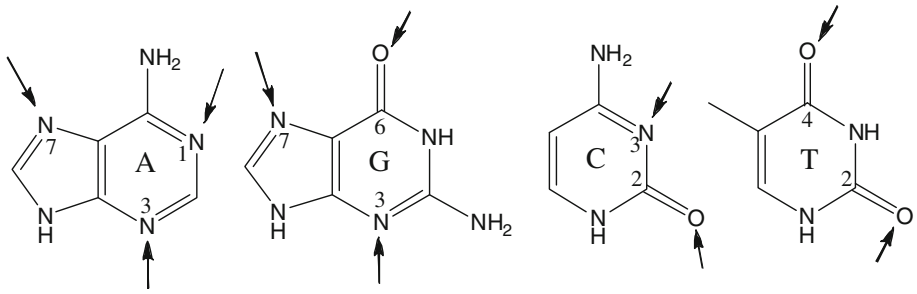

Fig. 10 Drawing of unprotonated nucleobases in their preferred tautomeric forms showing binding sites for metal cations. Metal binding sites include N1, N3 and N7 sites in adenine; N3, N7 and O6 sites in guanine; N3 and O2 in cytosine; and O2 and O4 sites in thymine/uracil

ligand of a metal complex, such as $Ru(phen)_2Cl_2$, $[Ru(phen)_3]^{2+}$, $[Zn(phen)_3]^{2+}$ [46–48], and the heterocyclic nucleobases by intercalation or shape-selective binding to the grooves employing week forces such as van der Waals interactions. Direct bonding involves the interaction between the filled orbital of the ligand atom of a nucleobase and a suitable, empty orbital of the metal ion.

Metal ion-phosphate interaction is an important interaction contributing to the stability of B-DNA and involves the coordination of positively charged metal ion and the negatively charged phosphate backbone and is characterized by an approximate metal-phosphate distance >7 Å. Usually, sodium and potassium ions serve as bulk electrolytes in this mode of binding. However, divalent and trivalent metal cations bind more tightly due to greater charge density. Therefore, Mg^{2+} serves second to K^+ in intracellular concentration as counterion for the phosphate groups of nucleic acids in cell [49].

The N7 sites of purines are exposed in all polymorphic forms of DNA and therefore represent excellent metal binding sites. Theoretical as well as experimental results indicate that metal binding to N7 site of purines can strengthen base pairing [50]. Binding to donor atoms in the minor groove creates stereochemical restrictions on the positioning of the co-ligands at the metal entity, because metal has to be inserted into a relatively narrow groove generated by two anti-parallel strings of sugar-phosphate backbones [21].

The unprotonated endocyclic N-atoms and exocyclic carbonyl O-atoms of nucleobases in their preferred amino and keto tautomeric forms are obvious metal binding sites (Fig. 10). These include N3, N7 and O6 sites in guanine; N3 and O2 in cytosine; N1, N3 and N7 sites in adenine and O2 and O4 sites in thymine/uracil. The exocyclic amino groups, although having a lone pair on N-atom, are not usually a useful metal binding sites due to the delocalization of the lone pair into heterocyclic ring, which leads to very low basicity [51].

7.1 Spectroscopic Evidence of DNA-Metal Ion Interaction

Metal ion association with DNA will perturb the electronic environment of the surrounding nuclei due to electron withdrawing effects and structural changes. NMR spectroscopy has been used extensively to probe metal ion association and its effects on DNA structure. There is spectroscopic evidence that allows in some cases to pinpoint the nature of DNA-metal ion interactions.

For example, ^{13}C NMR spectroscopy shows that the metallation of G_{N7} by Zn^{2+} induces downfield shifts of G_{C8} and upfield shifts of G_{C4} and G_{C5}. Significant ^1H NMR chemical shifts (Fig. 11) followed by disappearance of thymine N3H resonance on addition of Hg^{2+} confirms the selective binding of Hg^{2+} to T_{N3} [52, 53]. Cation association with the phosphodiester backbone generally will results in a downfield shift in the ^{31}P NMR due to deshielding

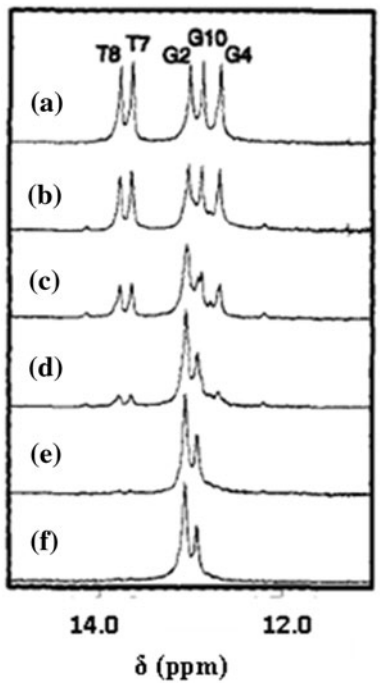

Fig. 11 ^1H NMR spectroscopy of the interaction between the oligonucleotide $[d(CGCGAATTCGCG)]_2$ and Hg(II). In the imino region of the ^1H spectrum, the thymine N3H resonances disappear upon Hg(II) addition, showing that Hg(II) presumably interferes with the Watson–Crick A–T hydrogen bonding. There is perturbation in guanine imino protons but no coordination between guanine and Hg occurred. The Hg(II) concentrations were: (*a*) 0, (*b*) 6, (*c*) 13, (*d*) 19, (*e*) 15, and (*f*) 28 mM. "Reprinted with permission from Froeystein and Sletten [53]"

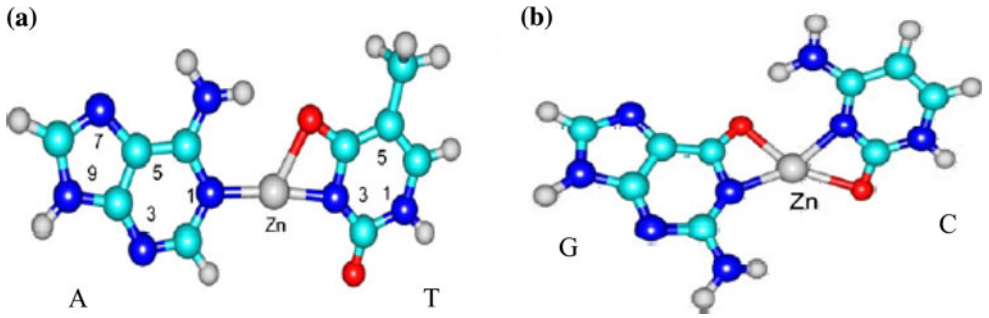

Fig. 12 3D structural models of the coordination of Zn^{2+} ions with the endocyclic nitrogen and exocyclic carbonyl oxygen atoms of DNA bases. **a** $ATZn^{+}$ complex, A_{N1}-Zn-T_{N3O4}, the dihedral angle between planes of the bases being 176.1°. **b** $GCZn^{+}$ complex, G_{N1O6}-Zn-C_{N3O2}. With kind permission from Springer Science + Business Media: Rubin et al. [106], Fig. 1." When metal cations crosslinked the nucleobases in opposite strands, they displace the bases from one another and coordinate with their endocyclic nitrogen and exocyclic carbonyl group

Table 3 Perturbations of selected Raman bands of DNA in divalent metal complexes

	160 bp fragments of calf thymus DNA		>23 kbp fragments of calf thymus DNA	
	Backbone 100-% δ_{834}	C = O % δC = O	Backbone 100-% δ_{834}	C = O % δC = O
DNA	100		100	
SrDNA	85 ± 9	9 ± 8	91 ± 21	20 ± 17
BaDNA	83 ± 10	10 ± 9	82 ± 29	14 ± 23
MgDNA	93 ± 9	12 ± 8	91 ± 19	13 ± 15
CaDNA	82 ± 12	15 ± 10	83 ± 18	14 ± 15
MnDNA	77 ± 11	13 ± 10	36 ± 14	58 ± 11
CdDNA	78 ± 13	36 ± 11	41 ± 15	56 ± 12
NiDNA	63 ± 8	24 ± 7	31 ± 13	71 ± 11
CoDNA	47 ± 14	36 ± 13	–	–
CuDNA	–	–	45 ± 20	46 ± 21
PdDNA	–	–	0 ± 17	106 ± 14

Symbols: δ and % δ represent absolute and percentage changes, respectively, in band intensity. C=O is the complex carbonyl band in the 1650–1680 cm^{-1} interval. $\delta\sigma$ is the absolute frequency (cm^{-1}) shift of the indicated band, *I* represent peak height. Values adapted from Duguid et al. [54]

effect. Upfield shifts have been observed which indicate metal induced structural perturbation but may not necessarily be indicative of the exact site of metal coordination. Duguid et al. [54] comprehensively studied the interactions of divalent metal cations with calf-thymus DNA (>23 kilobase pairs) and mononucleosomal fragments (160 base pairs) of DNA by laser Raman spectroscopy. Their study concluded that the transition metal cations (Mn^{2+}, Co^{2+}, Ni^{2+}, Cu^{2+}, Pd^{2+} and Cd^{2+}) induce the greatest changes in B-DNA structure, which include slight disordering of the B-form backbone, a decrease in base stacking and base pairing, and specific interactions between metal ions and the N7 of purines and the N3 of pyrimidine bases. This becomes very relevant when discussing cis-platin interactions with DNA (vide infra). Moreover, metal ions are involved in crosslinking the nucleobases of denatured DNA. The base to phosphate binding affinity was found to be $Pd^{2+} > Cu^{2+}$, $Co^{2+} > Ni^{2+}$, Cd^{2+}, $Mn^{2+} > Ca^{2+} > Mg^{2+}$, Sr^{2+}, Ba^{2+}. Alternatively, metal interaction at a major groove site may in fact locally destabilize the B-DNA helix, which results in an outward twist of the nucleobases away from one another thereby exposing additional metal binding sites. The end result is crosslinking of the two DNA strands through metal ions and eventually formation of an extended network, resulting in aggregation. Raman study by Langlais et al. [55] revealed that particularly Zn^{2+} binds to the phosphate groups of DNA (calf thymus) at a small metal : phosphate ratio of 1:30. The affinity of Zn^{2+} and Cd^{2+} ions for G-C base pairs is similar, whereas the affinity of Cd^{2+} ions for A–T base pairs is higher than Zn^{2+}. Interstrand crosslinking was proposed through the N3 of pyrimidines in the presence of Zn^{2+}.The crosslinking models between the DNA nucleobases and metal cations (Zn^{2+}) ions are shown in Fig. 12. The perturbations of selected Raman bands of DNA in divalent metal complexes are given in Table 3.

UV absorption studies by Shin [56] and later by Bregadze [57] showed that metal ions interacting with DNA cause a bathochromic shift of the absorption band. In addition, changes in CD (Fig. 13) also confirm the interactions between metal ion and DNA. Evidence suggests the involvement of the water molecules of the aqua-ion in the interactions with the nucleobases. Metal ion concentration influences structure particularly at higher concentrations where a helical conformation is less stable than random coil structure. Metal binding to the nucleobase plays an important role.

For instance in case of Cu^{2+} and Cd^{2+}, the effects on single stranded as well as double stranded oligonucleotides are similar to those caused by an increase in temperature. Conformational changes of metal binding either to the phosphodiester backbone (Mg^{2+} and Ca^{2+}) or to both,

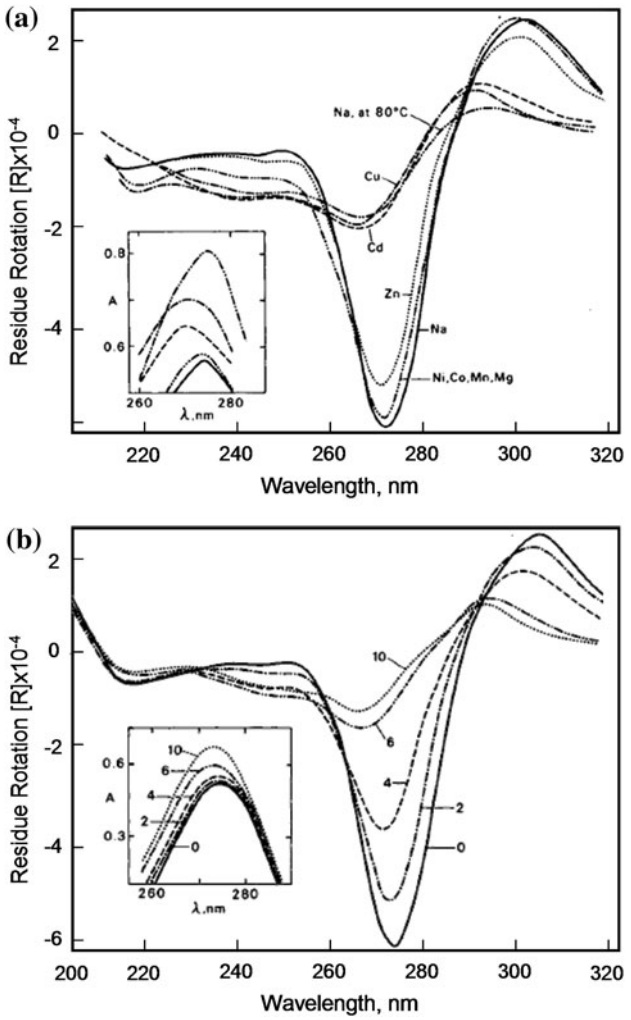

Fig. 13 **a** Effects of different metal cations on the CD spectrum of 10 mM poly(C) DNA and UV spectra (*inset*), include Na^{+}, Ni^{2+}, Co^{2+}, Mn^{2+}, Mg^{2+}, Zn^{2+}, Cd^{2+} and Cu^{2+}. Note: Zn^{2+} is in the middle of the effects caused by these metal cations. **b** Effect of the concentration of Zn^{2+} on the CD spectrum and UV spectra (*inset*), concentration ranges from 0–10 $\times$ 10^{-4} M indicated in the spectra. "Reprinted with permission from Wiley, Shin [56]" This comprehensive study by Shin on various DNA sequences and metal ions at various concentrations concluded that helix stabilization/destabilization by the metal ions depends on the particular nucleoside bases involved and the preferred conformation which a particular polymer tends to assume

nucleobases and the phosphodiesters (Zn^{2+}, Ni^{2+}, Co^{2+}, Mn^{2+}) are readily followed by spectroscopic means (see Fig. 13).

7.2 Stabilization and Destabilization Effects of Metal Ions on DNA

Metal ions (e.g. $\sim$2 mM Na^{+}) are necessary to stabilize the native structure of ds-DNA since it undergoes the unwinding process in distilled water. Moreover, the melting temperature (T_m) increases proportionally with log of

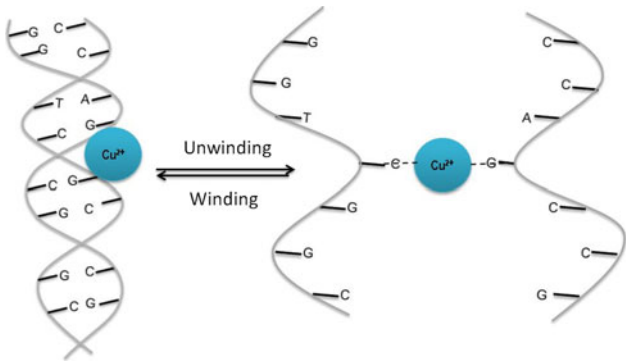

Fig. 14 Schematic view of the denaturation (*unwinding*) and renaturation (*winding*) of DNA in presence of Cu^{2+}. At room temperature, Cu^{2+} binds to the phosphate sites only, but at higher temperatures binding of the Cu^{2+} ions to nitrogen atoms of the nucleobases can occur causing significant distortion or partial disruption of the helix ultimately resulting in denaturation

ionic strength. Divalent cations are effective at much lower concentrations than univalent cations because of their higher binding tendency for the phosphate groups. For instance, Mg^{2+} has higher tendency towards phosphate, thus stabilizing the double helical structure by the counter ion effect, thus increases the T_m. However, not all the metal cations stabilize the DNA helix, for instance, less energy is required to melt the DNA helix in presence of Cu^{2+}. This is because Cu^{2+} not only binds to the phosphate but also accommodates nitrogen containing ligands of the nucleobase, which competes with H-bonding of the double helix and therefore facilitate the destabilization. Moreover, the competitive effect between H-bonding and Cu^{2+} binding can obtain a reversible unwinding and rewinding of DNA [58–61]. This effect is due to the formation of cross-links between the DNA strands by Cu^{2+} in denatured state. The cross-linking between the DNA strands mediated by the Cu^{2+} is depicted in Fig. 14.

Many metal ions bind to both phosphate and nucleobase sites, therefore their effect on DNA depends on their relative affinity for the two types of the binding sites. Evidently Mn^{2+}, Zn^{2+}, Cd^{2+} and Cu^{2+} give increasing T_m with initial increments in metal concentration due to phosphate binding at low concentration. After reaching a maximum T_m, further increase in metal concentration decrease T_m by breaking H-bonds of the nucleobases. Thus, Eichhorn and Shin [62] suggested on the basis of metal ion-DNA melting studies, Fig. 15, that the preference for phosphate over base association decreases in the order of Mg^{2+}>Co^{2+} = Ni^{2+}>Mn^{2+}>Zn^{2+}>Cd^{2+}>Cu^{2+} in Type I calf thymus DNA. Moreover, T_m decreases at high metal concentrations indicating that the presence of high concentration of divalent cation decreases the stability of DNA double helix structure. In addition, significant difference in T_m at same concentration of metal ions shows that every

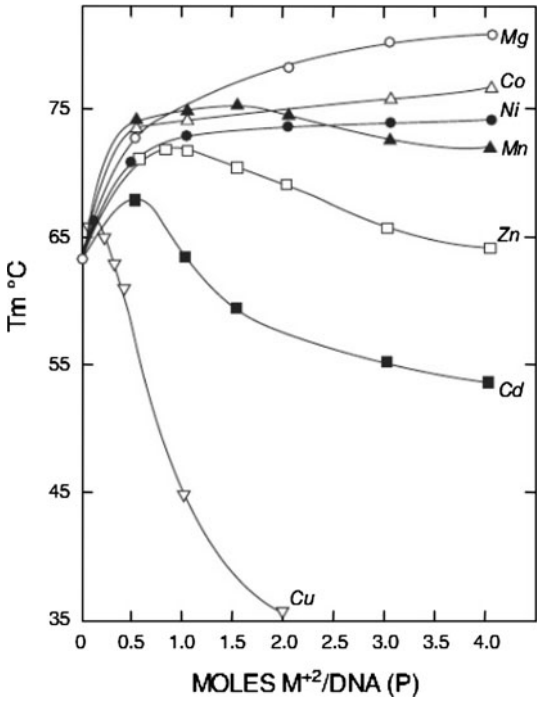

Fig. 15 Variation of melting temperature (T_m) of calf thymus DNA solutions as a function divalent metal ion concentration. "Reprinted with permission from Eichhorn and Shin [62]"

metal ion has different interaction with DNA. The reverse of this order can aptly be correlated with the effect of these metals on the rewinding of the unwound DNA in their presence, since this behaviour can be explained as an increasing relative affinity for nucleobase versus phosphate in this series. Interestingly, Souza [63] found in case of Zn^{2+}, the total entropy did not change significantly with the increase in metal ion concentration.

Since the effects of metal ions on the stability of DNA is probed by the thermal denaturation studies providing a melting temperature T_m, one has to be mindful that the T_m is affected by a multitude of factors including the base sequence, the DNA concentration, as well as the buffer. Thus, in order to carry out accurate comparisons of different metal–DNA systems, the base sequences used, the specific experimental conditions, thermal stability of the individual metal complexes, and their positioning along the DNA duplex must all be considered [64].

7.3 Site-Specific Metal Binding in DNA

There are reports that some metal ions are able to interact with nucleobases directly along the H-bonded interface. Lee and coworkers suggested the formation of such complexes as a result of interaction between the divalent metal ions Zn^{2+}, Ni^{2+} and Co^{2+} and B-DNA at pH 8.5 [65, 66]. This is marked by the disappearance of the imino proton signals in NMR. More direct studies have shown site-specific coordination of Hg^{2+} to the nitrogens between T–T mispairs.

Ono et al. [67] studied the ^{15}N NMR of the interaction between Hg^{2+} and T–T mispairs and found strong evidence of the structure of up to five T–Hg–T pairs in a row. Hg^{2+} binds with high preference to thymine bases in DNA hairpin loop structure and T–T mispairs in ds-DNA (Fig. 16a), which in turn enhances its thermal stability. This suggests that it might be possible to introduce metal ions into specific sites and construct metal-DNA constructs with a specific metal content. Subsequently, a number of studies appeared that used a combination of Cu^{2+} and Hg^{2+} to construct artificial DNA duplexes (see Fig. 16c, vide infra) [68]. Peferential binding of Ag^{+} to poly dG–dC [69] and to a C–C mispair have also been reported (Fig. 16b) [70].

Another important aspect of divalent metal ion interaction is the ability of metal ions to induce or prevent nucleic acid conformational transitions. It has been previously reported that such metals (Ca^{2+}, Mn^{2+}, and Cu^{2+}) in certain concentrations can prevent B → A transition in DNA while reducing DNA hydration [71, 72]. Metal ions can also induce double-to triple-strand transition and formation of triple helical structures of nucleic acids [73]. The double helix destabilization can be sequence specific [21]. Moreover, pH is key for the conformational change induced by metal ions on surface immobilized DNA, for instance, Zn^{2+} and Ni^{2+} were found to bring conformational change at pH 8.5 but not 7.5, while Mg^{2+} and Ca^{2+} had insignificant changes when exposed to immobilized 30 bp 50 % GC ds-DNA [74].

Trivalent as well as divalent ions acting synergistically with other factors can induce DNA condensation into highly condensed particles in vitro [75–78]. The condensation process plays a very important role in DNA packing in living cells [44]. Binding of metal ions to specific phosphate sites on RNA and DNA may induce folded conformations of branched DNA or RNA. For instance, Mg^{2+} has been reported to stabilize four-way helical (Holliday) junctions in DNA Fig. 17.

In summary, DNA and RNA are unique polymeric biomolecules which acquire distinct secondary structures (A, B, Z and Hoogsteen) depending on the environmental conditions (hydration, ionic strength, metal ions). These structures have canonical Watson–Crick and/or non-canonical Hoogsteen and wobble base pairs, mispairs and mismatched pairs, which are dynamic sites to interact with metal ions. The negatively charged phosphate backbone electrostatically attracts positively charged metal ions while nucleobases can interact with metal ions in a Lewis acid–base fashion. Some metal ions can bind specifically to the specific base pairs such as C–Ag^{+}-C and T-Hg^{2+}-T. Metal ions have characteristic impact on DNA stability and

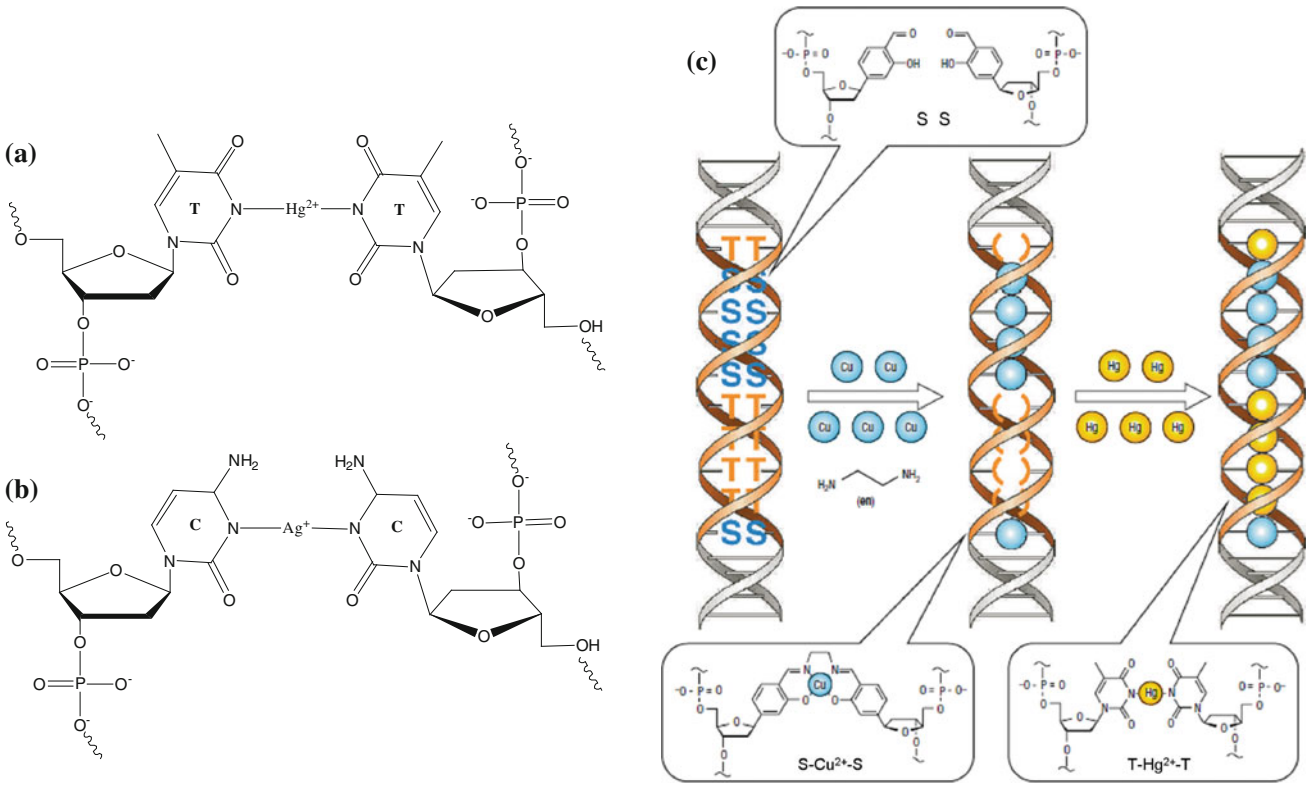

Fig. 16 Sites specific metal binding in DNA. **a** Hg^{2+} specifically binds to T–T mismatch through covalent bonding by replacing the H-atoms from the endocyclic N3 atoms of two thymine residues. **b** Ag^{+} also replaces the H-atoms from the endocyclic N3 atoms of two cytosine residues and specifically binds to C–C mismatch. **c** Programmable assembly of the metal ions (Cu^{2+} and Hg^{2+}) between DNA base pairs using salen modified nucleobases (S S) and mismatched (T T) nucleobases. Reprinted by permission from Macmillan Publishers Ltd: Tanaka et al. [69]

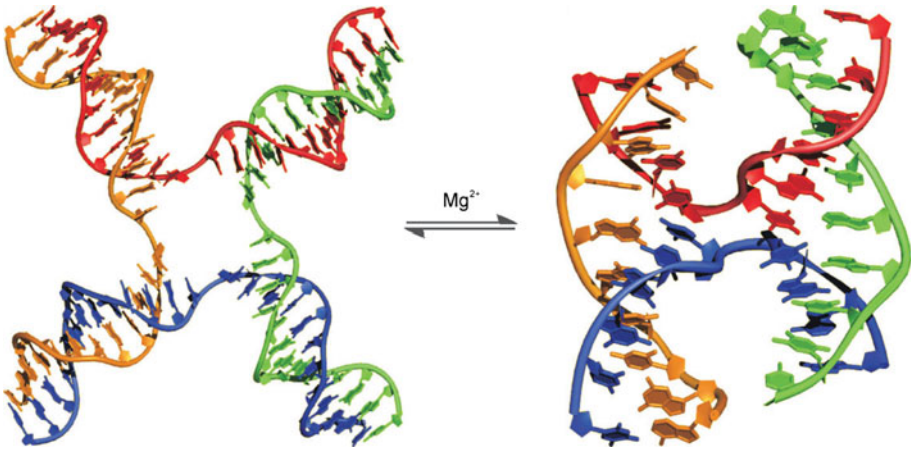

Fig. 17 Mg^{2+} stabilizes four-way helical (Holliday) junctions in DNA. Representative structures of DNA four-way junctions in an extended, unstacked conformation (*left*) and the stacked X conformation (*right*). "Reproduced from Müller [43] with permission of The Royal Society of Chemistry"

structure depending on the type of metal ion, concentration of metal ion, temperature and the relative affinity of the metal ion for the phosphate and nucleobases. In presence of the metal ions, DNA can also acquire higher order structures such as triplex and G-quadruplex structures. In next section of this review, a number of applications of metal ion-DNA interactions are described with relevance to the fields of nanotechnology, medicine, biosensor and bioelectronics.

8 Applications of DNA-Metal Ion Interactions

8.1 DNA-Metal Nanostructures

As was outlined above, metal ions or metallo-ligand attached to DNA can be used to promote DNA interactions. In fact, this has led to the use of DNA as a building-block for the assembly of nanostructures. The versatility of this approach has been discussed in detail elsewhere [64, 79],

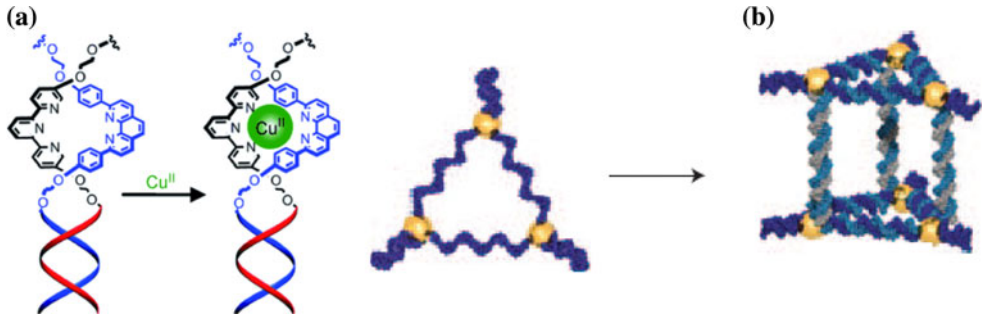

Fig. 18 A schematic representation outlining the assembly of a metallated 3D structure. **a** Incorporation of terpyridinephenanthroline modifications to DNA and the metal binding to form highly stable duplexes. Reproduced by permission from Wiley, Yang et al. Angew. Chem. Int. Ed. 2009, 48, 9919–9923. **b** Formation of DNA-metal cage (prism) using pre-metallated *triangles*. Reprinted by permission from Macmillan Publishers Ltd: Metal–nucleic acid cages, H. Yang, C.K. McLaughlin et al. 1, 390–396) copyright (2009)

however, few prominent examples are discussed here. In particular, the use of DNA conjugates in which a metal ligating site provide a building plan for complementary strand into 2D and 3D constructs was exploited by Sleiman and coworkers. A range of structures were obtained many of which display a surprising thermal stability at temperatures of up to 40 °C higher than the T_m of unmetallated DNA [80].

For example, using $(dpp)_2$–metal–DNA junctions, which provide to a 120° angular coordinative building block allows the construction of triangles and prisms [80]. This approach has also led to the development of structures that enable to make the transition from the nanoscopic into the macro-level, which shows the tremendous potential of this approach for the construction of molecularly designed macroscopic objects [81] (Fig. 18).

The substitution of the Watson–Crick base pairs by metal complexes has shown great promise in molecular wire development. This was due to the creation of metal–base pairs, which may potentially incorporate magnetic and conductive properties into DNA-based nanostructures. Thus, there is a hope that DNA-based molecular wires will provide biocompatible electrical conduction at the interface between electronic circuits and biological systems (such as nerve cells). Here, the most recent and prominent development in this area will be discussed.

Shionoya's group [82] incorporated five consecutive copper–hydroxypyridone base pairs (S-Cu–S) into a double strand (Fig. 19a). It is interesting to note that EPR evidence suggests ferromagnetic coupling between the Cu(II) centers. Recently, Shionoya group [68] synthesized DNA strands possessing a programmed sequence by the automated solid phase synthesis. This sequence contains five salen ligands 'S' which can bind to Cu(II) and five T–T mismatches having high affinity for Hg(II) as shown in Fig. 16c. CD-spectroscopic titration studies confirmed the incorporation of the right number of Cu(II) and Hg(II) ions according to the programmed sequence. Similarly, Clever and Carell exploited salen chemistry for aligning up to ten Mn^{3+} ions along the duplex [83]. Müller and co-workers [84] demonstrated the self-complementary DNA oligonucleotide with three consecutive imidazole nucleotides in its centre using NMR solution structure. The hairpin structure (Fig. 19b) is adopted by the artificial nucleotides forming the loop in the absence of metal ions with, which turns into a duplex in the presence of Ag(I) ions with three imidazole–Ag^+–imidazole base pairs in the centre Fig. 19b. The B-type conformation was observed with slight deviations in the centre. Clearly, there is tremendous potential in metallated DNAs, in particular with respect to the design of molecules with specific electric properties.

8.2 Medicinal Applications of Metal Complexes

Platinum metal complexes have found some application in anti-cancer therapy and other metal complexes are currently undergoing clinical trials. While this review will not outline this work in detail it is important to describe the concepts. Recently, Pizzaro and Sadler have reviewed not only Pt complexes but also complexes of Zn, Ti, Ru, Rh, Os and Au for their antiviral and antitumor activity [85]. Here, we briefly discuss some important metal complexes in regards to their activity as anticancer and antiviral agents.

Only a handful of Pt complexes are approved for anticancer treatment worldwide, including cisplatin, carboplatin and oxaplatin (Fig. 20). Some other complexes are approved in some jurisdictions only (nedaplatin in Japan, lobaplatin in China and heptaplatin in South Korea) [76].

Jamieson and Lippard have reviewed various cisplatin analogues and the structure, recognition, and processing of the DNA-cisplatin adducts [86]. There are five known types of DNA-cisplatin crosslinking adducts that form upon interactions, as depicted in Fig. 21a. Among these adducts, the 1,2-intrastrand d(GpG) adduct comprises about 65 % of the total adducts while the 1,2-intrastrand

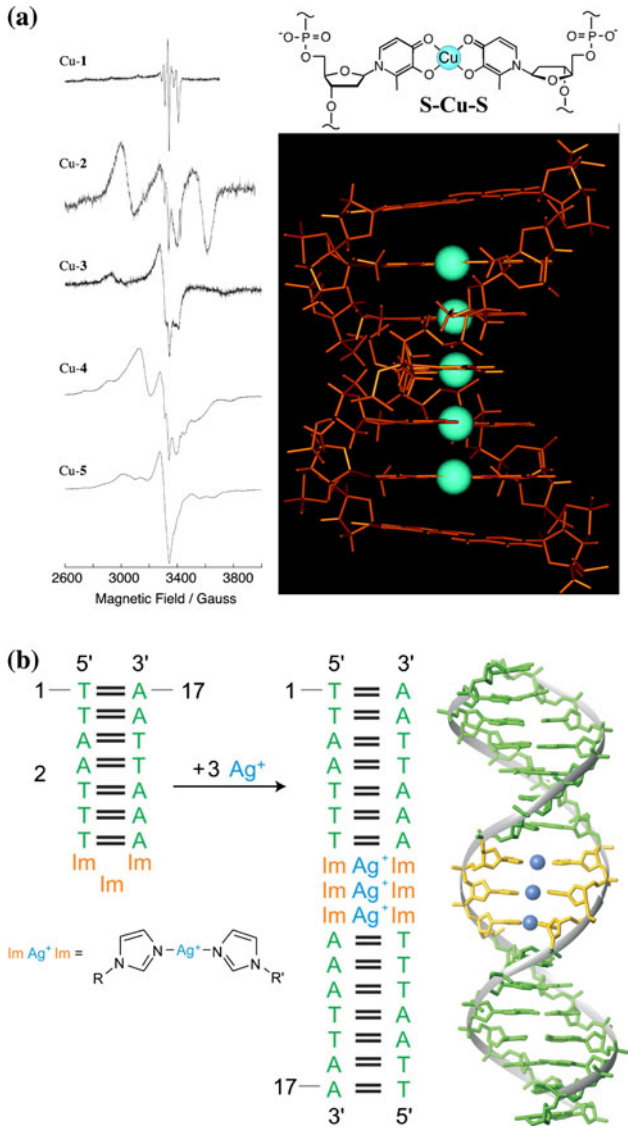

Fig. 19 **a** CW-EPR spectra of the duplexes Cu–n ($n = 1$–5) In a frozen aqueous solution at 1.5 K with a 9.5-GHz microwave for an incorporated five consecutive copper–hydroxypyridone base pairs (S-Cu–S) into a double strand shown in right. "From Tanaka et al. [83]. Reprinted with permission from AAAS." **b** In left, schematic depiction of the hairpin-to-duplex transition of the oligonucleotide and in right, lowest-energy structure of the duplex containing Ag^+-mediated imidazole base pairs in the centre. The natural A–T base pairs are coloured in green, the imidazole nucleobases in gold, and Ag^+ ions are shown as blue spheres. Reprinted by permission from Macmillan Publishers Ltd, Johannsen et al. [85]

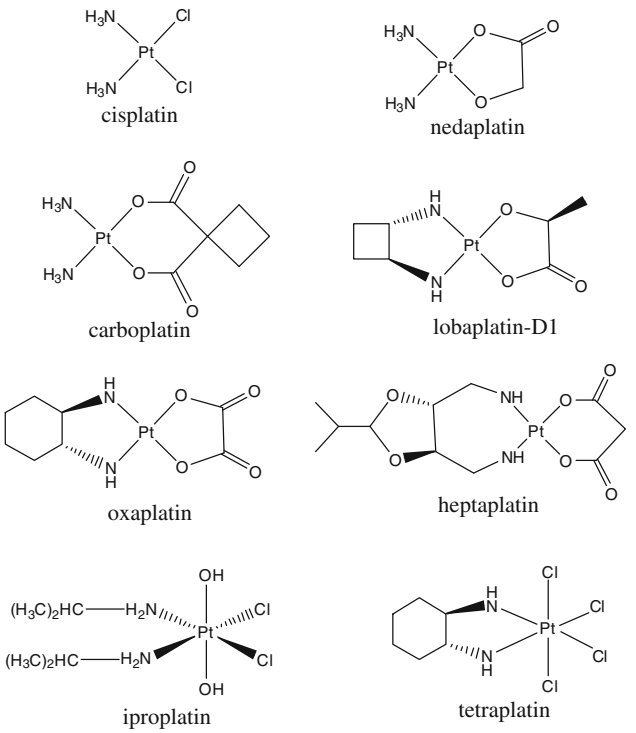

Fig. 20 Platinum drugs. Cisplatin, carboplatin and oxoplatin have been approved by FDA in 1978, 1989 and 2002 respectively for clinical use. Nedaplatin, iobaplatin and heptaplatin have been approved in Japan, China and South Korea, respectively

d(ApG) adduct makes up about 25 %. 1,3-intrastrand d(GpNpG) and 1,2-interstrand GpG and monofunctional adducts appear unfavourable and make up less then 10 %. (See crystal structure in Fig. 21b).

DNA chelation gives rise to specific distortions (e.g. bending or kinking) of the duplex, which is a critical lesion resulting in a breakdown of biomolecular recognition and failure to ultimately transcribe the DNA. It is interesting to note here that Pt(IV) complexes such as iproplatin and tetraplatin, in contrast to Pt(II) cisplatin and its analogues, are potentially promising drug since Pt(IV) complexes are octahedral and less susceptible to substitution reactions. This in turn lowers their toxicity and may increase activity.

The limitations of the platinum-based drugs due to their effectiveness for certain tumours and their toxic side effects have fuelled the development of improved metal-based drugs in recent years. Two prominent Ru based anticancer compounds, i.e. KP1019 [88], NAMI-A [89], have entered clinical trials and are at different phases of their trial. Figure 22 shows some metal complexes of different metal ions that have entered clinical trials.

8.3 Biosesensor for DNA Mismatch Detection

Hybridization events in DNA can be monitored using labels or using label-free techniques. Former requires labelling of the probe or target sequence with small molecules, like fluorophores, which can generate or amplify the physically measurable signal. Recently, there is a burgeoning interest in the electrochemical methods for mismatch detection in DNA due to intrinsic high sensitivity and capability of being miniaturized.

A basic electrochemical sensor consists of oligonucleotide strands on a transducer surface, which act as

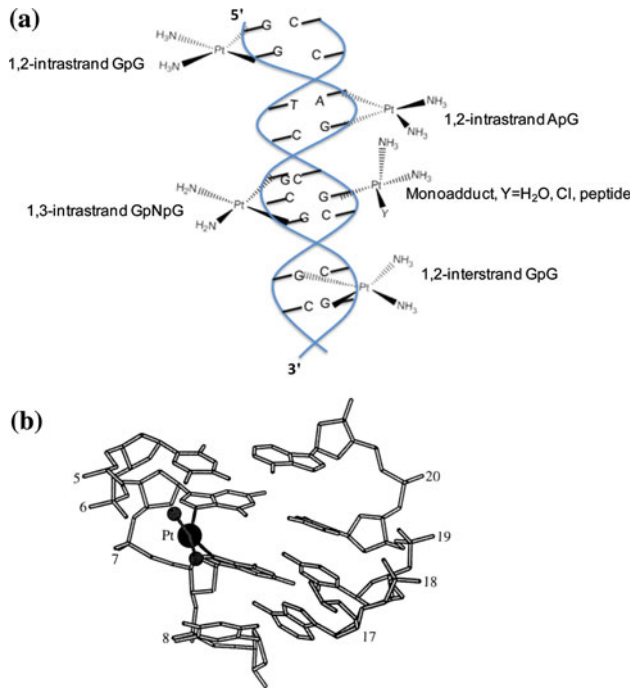

Fig. 21 **a** Types of DNA-cisplatin crosslinks. 1,2-intrastrand d(GpG) adduct (~65%); 1,2-intrastrand d(ApG) adduct (~25%); 1,3-intrastrand d(GpNpG), 1,2-interstrand GpG and monofunctional adducts (<10%). **b** X-ray crystal structure at 2.6 Å resolution of the 1,2-intrastrand GpG adduct formed between cisplatin and double stranded d(CCTCTG*G*TCTCC). "Reprinted by permission from Macmillan Publishers Ltd: [Nature] (Crystal structure of double-stranded DNA containing the major adduct of the anticancer drug cisplatin, Takahara et al. 377, 649–652), copyright (1995)." This study shows the X-ray crystallographic study of the first double stranded DNA and cisplatin adduct in a 12-mer DNA

capture strands. The event of hybridization between capture strands and the incoming target strands is detected and transformed into a current signal [90]. Some metal ions can recognize the specific types of mismatches, such as Hg^{2+} and Ag^{+}, which have a strong affinity for T–T and C–C mismatches, respectively [91, 92]. Such recognition changes structural conformation which may not be ideal for sensing multiple events. However, Zn^{2+} was reported to be a useful for signal amplification without causing structural deformation.

In metal-ion approach, the microscopic properties of the DNA films were exploited on gold surfaces. In detail, the solution based negative redox probe, $[Fe(CN)_6]^{3-/4-}$, experiences resistance in charge transfer (R_{CT}) at the interface when reaching the electrode surface. The resistance is due the DNA film itself and the negative charge on the backbone of DNA. However, addition of metal ion, in this case Zn^{2+}, facilitates the charge transfer thus reducing the R_{CT} (Fig. 23a). Such facilitation of the charge transfer is caused by the higher penetration of the redox probe due to negative charge neutralization. Electrochemical impedance spectroscopy (EIS), a powerful technique, gives detailed information about the interface (solution/ds-DNA/electrode) in the form of capacitative and resistive components through fitting Randle's equivalent circuitry (Fig. 23b).

Interestingly, the difference in charge transfer resistance (ΔR_{CT}), before and after the addition of Zn^{2+} into ds-DNA film, is dependent on the type of DNA film, thus easily discriminates the matched and mismatch containing films. The ΔR_{CT} is higher for matched than mismatch DNA films,

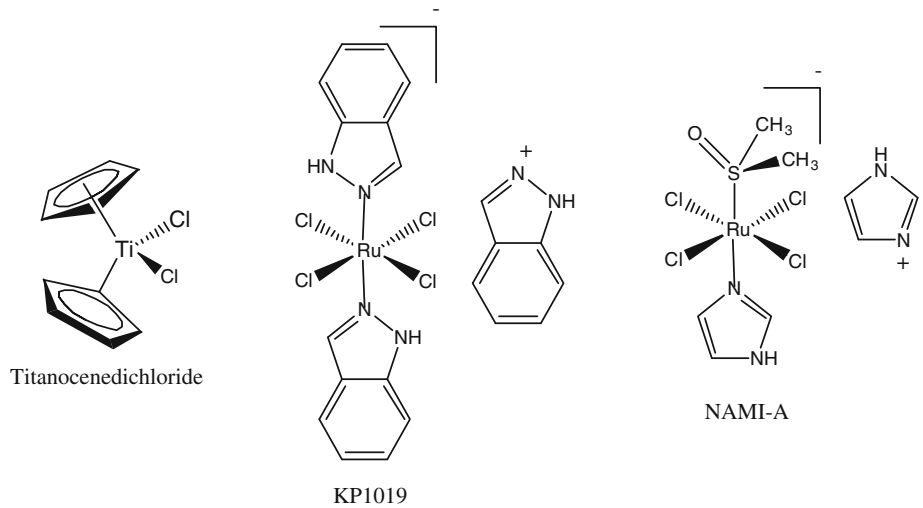

Fig. 22 Chemical structures of metal-containing antitumor drugs which were/are considered for clinical trials. The detailed antitumor activity of titanocene dichloride was studied by Köpf and Köpf-Maier [87]. It entered phase II trial in 2000 but its efficacy rate with metastatic renal cell carcinoma and metastatic breast cancer were too low to support further evaluation of the drug. KP1019 was developed by Keppler and coworkers in Vienna and NAMI-A was developed in Mestroni's lab in Trieste. Both drugs are currently undergoing clinical trials [80]

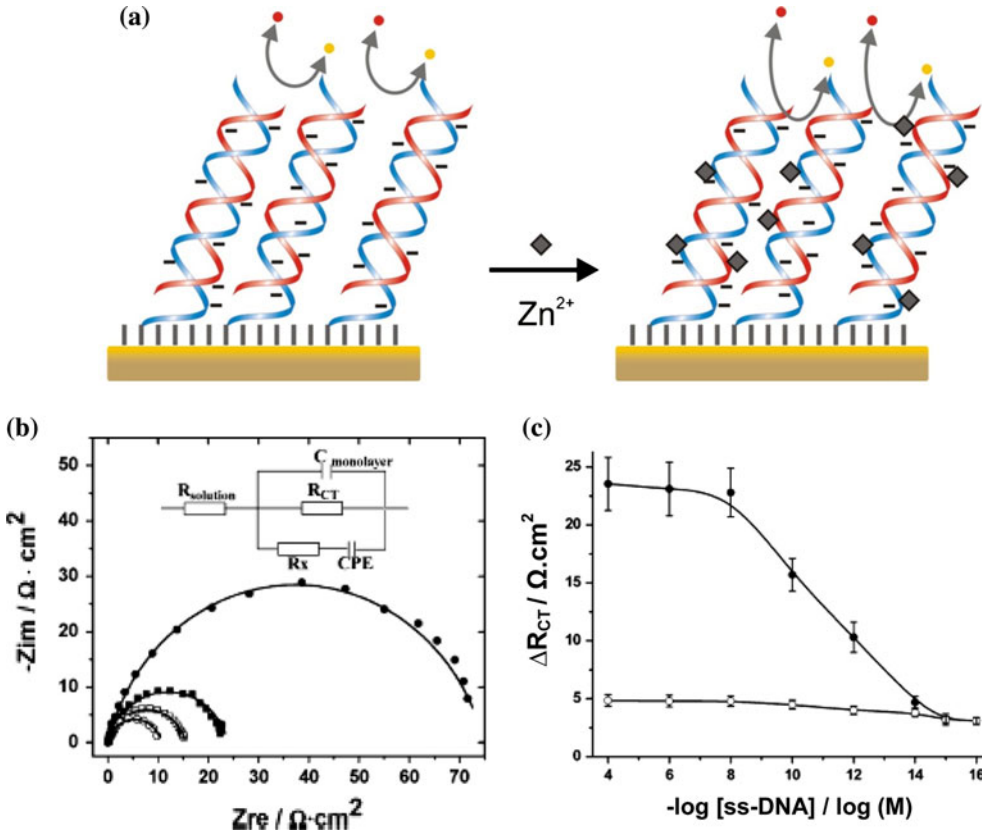

Fig. 23 **a** Schematic representation depicting the electron transfer process across the surface immobilized ds-DNA film between the negative redox probe $[Fe(CN)_6]^{3-/4-}$ and gold transducer surface. Electron transfer process is facilitated by the addition of metal ion (Zn^{2+}) that neutralizes the phosphate backbone of DNA and allows the enhanced diffusion of the redox probe. As a result the differences in charge transfer resistance R_{ct} before and after the addition of metal ion are significantly different and are in fact affected by the presence of a single nucleotide mismatch. **b** Nyquist plot showing the charge transfer resistance across a matched and a mismatched film in absence and presence of Zn^{2+} in the form of semicircle. *Inset* shows the modified Randle's equivalent circuit used to fit the data. **c** The plot showing the detection limit of the system as low as 10 fM. Reproduced with permission from Li et al. [93]

which is consistent irrespective of the length of DNA strand, type of mismatch, position of mismatch and number of mismatches in DNA. Presumably, the fully matched DNA forms high order and uniform film, due to which they are less penetrable to redox probe. On the other hand, mismatch containing DNA films lack uniformity due to wobbled structure at the molecular level, thus, more penetrable and the difference is not higher after Zn^{2+} addition. It is important to note here that the Zn^{2+} binding in this approach is reversible, and the R_{CT} of the native DNA can be easily restored after washing the film in buffer [93], which asserts that the key role of the Zn^{2+} to phosphate binding. This approach can detect single nucleotide mismatches down to 10 fM level (Fig. 23c). The method has been tolerant to nonspecific adsorption of protein contaminations and also to heterozygote DNA mixtures [94].

This simple approach has also a promising application in an array format and has allowed detecting a range of different mismatches as well as at different positions. [95–97]. The array formed by the matched and mismatches containing ds-DNA films on gold substrate is interrogated using SECM in the presence of a solution based redox probe, Fig. 24a. The redox mediator, $[Fe(CN)_6]^{3-}$, generated at the tip of the electrode undergoes a reduction to $[Fe(CN)_6]^{4-}$ at the gold substrate, thus increasing the SECM feedback current on bare gold. In the vicinity of the ds-DNA film (Fig. 24b), the regeneration of the $[Fe(CN)_6]^{4-}$ at the substrate is considerably hindered by the electrostatic repulsion between the anionic redox probe and the negatively charged phosphates of the DNA chains, thus obtaining negative feedback current (Fig. 24c). In the absence of base pair mismatches, a ds-DNA film is generally well-packed and effectively blocks the diffusion of the redox mediator into the film, which lowers the SECM feedback current. The distinguishable differences in ds-DNA films, matched and mismatched, can be observed in the presence of Zn^{2+} due to variability in their diffusibility based on the film structure (Fig. 24d).

Scanning electrochemical microscopy (SECM) studies were critical to elucidate the mechanism of this process and

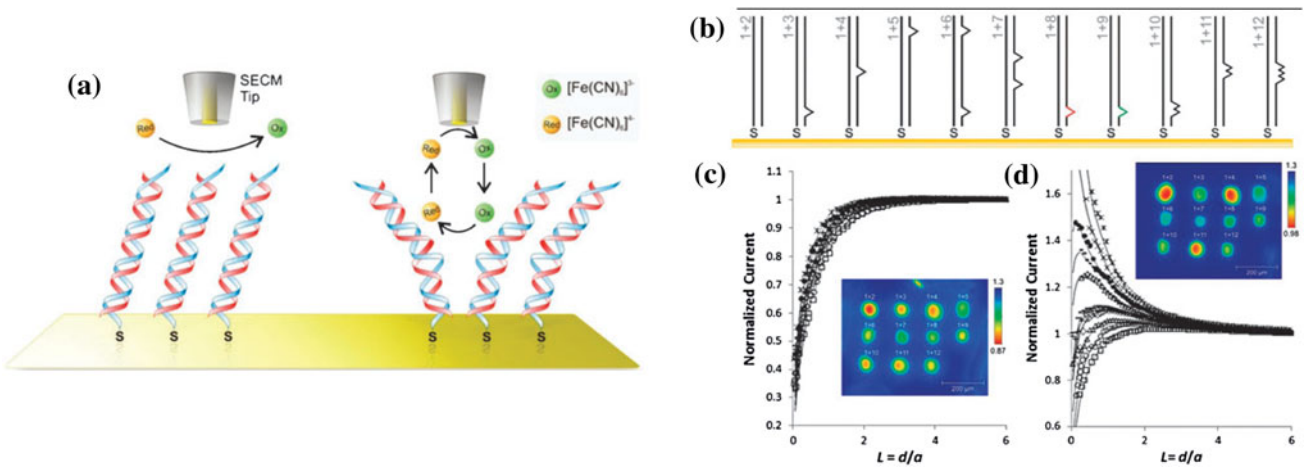

Fig. 24 **a** Schematic shows the redox cycling of the redox probe between the tip electrode and the matched (*left*) and a mismatched (*right*) DNA modified gold substrate. **b** Depicting the fully matched and mismatch containing films at different positions. SECM images and feedback current before (**c**) and after (**d**) the addition of Zn^{2+}. Reproduced from Diakowski and Kraatz [99] with permission of The Royal Society of Chemistry

rationalize the differences in R_{CT} in terms of the diffusive properties of the probe molecules [98, 99]. The heterogeneous electron transfer constants were evaluated in the proximity of the DNA film using SECM and it was shown that the k_{et} increases from 4.6×10^{-7} cm/s to 5.0×10^{-6} cm/s after the addition of Zn^{2+}. Recently, both EIS and SECM have shown strong potential towards the application for species identification [100, 101].

8.4 Nanoelectronics

There have been considerable contradictory discussions on the conductivity of DNA; reporting insulating, semiconducting, highly conductive, and even superconducting behaviour for the DNA molecule. Contradictions in the reports have been, perhaps, due to their unique experimental setups. Bearing in mind that alteration in the local environment of the DNA molecule causes the structural changes that can influence both the electronic structure and the conductivity of DNA [102]. Nevertheless, achievement of the metallic conductivity of the metal (e.g. Ag^{+}, Ni^{2+}, Zn^{2+}) doped DNA gained great attention of experimental as well as theoretical investigators [103]. Variety of DNA metal doping strategies has been adopted in the hope of producing good molecular wires or nanowires [83, 104]. Theoretical studies have been focusing upon the alteration in electronic and molecular structure of the interaction between the metal ion and the DNA bases by varying the type of cation in the structure of DNA, and calculating the energy values of altered HOMO and LUMO [105–107]. The key role of alkaline pH $\sim$8.5 has been consistently noticed for the effective interaction between the DNA base pairs to show metallic conduction, while DNA-metal ions conjugates are highly insulator at low pH [108].

9 Conclusions

Metal ions can interact with a range of binding sites on DNA and RNA. In B-DNA, some interactions, like those with Mg^{2+} are necessary to stabilize the B-form of DNA. In some cases, DNA-metal ion interactions trigger conformational changes. Clearly metal-DNA interactions are critical to interfere with biological processes. Cisplatin is a success story of a metal complex interaction having therapeutic value. A new generation of anticancer drugs based on other transition metals with less serious side effects is being developed and are currently undergoing clinical trials.

Non-natural nucleobases and ligand conjugation have allowed to exploit metal–ligand templating to construct nanoscopic objects with metal ions in predetermined positions. This will have tremendous impact for the design of new biomaterials with specific electronic properties, while maintaining the potential for biorecognition. Linked to surfaces, DNA films have enabled the construction of sensor systems that are able to discriminate single nucleotide mismatches at ultralow concentrations. This is very promising for the wide biosensing applications. Clearly, DNA-metal ion interactions are promising offering solutions to current and future problems.

References

1. V.V. Andrushchenko, VCD and IR spectroscopic study of metal ion induced structural changes of synthetic and natural nucleic acids at different temperatures (PhD thesis, University of Calgary, 2000) p. 1
2. N.V. Hud, *Nucleic acid-metal ion interactions* (RSC Publishing, Cambridge, 2009)

3. N. Hadjiliadis, E. Sletten, in *Metal Complex–DNA Interactions* (Wiley, Chichester, 2009)
4. *Interaction of Metal Ions with Nucleotides, Nucleic Acids, and Their Constituents*, ed. by A. Sigel, H. Sigel. Metal Ions in Biological Systems, vol 32 (Marcel Dekker Inc., New York, 1996)
5. S. Aoki, E. Kimura, Chem. Rev. **104**, 769 (2004)
6. J.D. Watson, F.H.C. Crick, Nature **171**, 737 (1953)
7. A.J. Brookes, Gene **234**, 177 (1999)
8. C.A. Hunter, K.R. Lawson, J. Perkins, C.J. Urch, J. Chem. Soc., Perkin Trans. **2**, 651 (2001)
9. S. Neidle, *Principles of Nucleic Acid Structure*, 1st edn. (Academic Press, Boston, 2008), pp. 38–80
10. Z. Shakked, G. Guerstein-Guzikevich, M. Eisenstein, F. Frolow, D. Rabinovich, Nature **342**, 456 (1989)
11. P. Belmont, J.-F. Constant, M. Demeunynck, Chem. Soc. Rev. **30**, 70 (2001)
12. R.E. Franklin, R.G. Gosling, Nature **172**, 156 (1953)
13. A.H.-J. Wang, G.J. Quigley, A. Rich, Nucl. Acids Res. **6**, 3897 (1979)
14. F.M. Pohl, T.M. Jovin, J. Mol. Biol. **67**, 375 (1972)
15. W. Zacharias, A. Jaworski, R.D. Wells, J. Bacteriol. **172**, 3278 (1990)
16. M.A. Fuertes, V. Cepeda, C. Alonso, J.M. Perez, Chem. Rev. **106**, 2045 (2006)
17. *A-DNA Duplexes in the Crystal*, ed. by S. Neidle. Oxford Handbook of Nucleic Acid Structure (Oxford University Press, Oxford, 1999)
18. B. Spingler, C. Da Pieve, Dalton Trans. 1637 (2005)
19. N.G.A. Abrescia, A. Thompson, T. Huynh-Dinh, J.A. Subirana, Proc. Natl. Acad. Sci. USA **99**, 2806 (2002)
20. J. Nowakowski, I.J. Tinoco, *RNA Structure in Solution*, in Oxford Handbook of Nucleic Acid Structure, ed. By S. Neidle, Oxford University Press, UK, 1999
21. P. Modrich, Ann. Rev. Biochem. **56**, 435 (1987)
22. O. Kennard, J. Biomol. Struct. Dyn. **3**, 205 (1985)
23. G. Kneale, T. Brown, O. Kennard, D. Rabinovich, J. Mol. Biol. **186**, 805 (1985)
24. D. Rabinovich, T. Haran, M. Eisenstein, Z. Shakked, J. Mol. Biol. **200**, 151 (1988)
25. W.N. Hunter, T. Brown, O. Kennard, Nucl. Acids Res. **15**, 6589 (1987)
26. V.A. Roongta, C.R. Jones, D.G. Gorenstein, Biochemistry **29**, 5245 (1990)
27. D.J. Patel, S.A. Kozlowski, S. Ikuta, K. Itakura, K. Itakura, Biochemistry **23**, 3218 (1984)
28. J.M. Benevides, A.H.J. Wang, G.A. Van der Marel, J.H. Van Boom, G.J. Thomas Jr, Biochemistry **28**, 304 (1989)
29. D.G. Gorenstein, S.A. Schroeder, J.M. Fu, J.T. Metz, V.A. Roongta, C.R. Jones, Biochemistry **27**, 7223 (1988)
30. E.O. Otokiti, R.D. Sheardy, Biochemistry **36**, 11419 (1997)
31. H. Urakawa, P.A. Noble, S. El Fantroussi, J.J. Kelly, D.A. Stahl, Appl. Environ. Microbiol. **68**, 235 (2002)
32. F. Aboul-Ela, D. Koh, I. Tinoco Jr., F.H. Martin, Nucl. Acids Res. **13**, 4811 (1985)
33. J. SantaLucia Jr., H.T. Allawi, P.A. Seneviratne, Biochemistry **35**, 3555 (1996)
34. H. Werntges, G. Steger, D. Riesner, H.-J. Fritz, Nucl. Acids Res. **14**, 3773 (1986)
35. T. Brown, O. Kennard, G. Kneale, D. Rabinovich, Nature **315**, 604 (1985)
36. D. Hare, L. Shapiro, D.J. Patel, Biochemistry **25**, 7445 (1986)
37. R. Kolodner, Genes Dev. **10**, 1433 (1996)
38. M. Yang, M.E. McGovem, M. Thompson, Anal. Chim. Acta **346**, 259 (1997)
39. K.J. Skogerboe, Anal. Chem. **67**, 449 (1995)
40. R.M. Izatt, J.J. Christensen, J.H. Rytting, Chem. Rev. **71**, 439 (1971)
41. I. Sissoeff, J. Grisvard, E. Guille, Prog. Biophys. Mol. Biol. **31**, 165 (1976)
42. I. Rouzina, V.A. Bloomfield, Biophys. J. **74**, 3152 (1998)
43. J. Müller, Metallomics **2**, 318 (2010)
44. M. Gellert, M.N. Lipsett, D.R. Davies, Proc. Natl. Acad. Sci. USA **48**, 2013 (1962)
45. B. Lippert, J. Chem. Soc., Dalton Trans. 3971 (1997)
46. J.K. Barton, E. Lolis, J. Am. Chem. Soc. **107**, 708 (1985)
47. J.K. Barton, A.T. Danishefsky, J.M. Goldberg, J. Am. Chem. Soc. **106**, 2172 (1984)
48. J.K. Barton, J.J. Dannenberg, A.L. Raphael, J. Am. Chem. Soc. **104**, 4967 (1982)
49. A. Sigel, H. Sigel (eds.) *Metal Ions in Biological Systems*, vol. 32 (Marcel Dekker Inc., New York, 1996), pp. 1–26
50. J. Sponer, J. Burda, M. Sabat, J. Leszczynski, P. Hobza, J. Phys. Chem. A **102**, 5951 (1998)
51. B. Luici, M. Orozco, J. Sponer, F.J. Luque, Z. Shakked, J. Mol. Biol. **279**, 1123 (1998)
52. P.R. Young, U.S. Nandi, N.R. Kallenbach, Biochemistry **21**, 62 (1982)
53. N.A. Froeystein, E. Sletten, J. Am. Chem. Soc. **116**, 3240 (1994)
54. J. Duguid, V.A. Bloomfield, A.J. Benevides, G.J. Thomas Jr., Biophys. J. **65**, 1916 (1993)
55. M. Langlais, H.A. Tajmir-Riahi, R. Savoie, Biopolymers **30**, 743 (1990)
56. Y.A. Shin, Biopolymers **12**, 2459 (1973)
57. V.G. Bregadze, Int. Jr. Quantum Chem. **17**, 1213 (1980)
58. S. Hiai, J. Mol. Biol. **11**, 672 (1965)
59. J.H. Coates, D.O. Jordan, V.K. Srivastava, Biochem. Biophys. Res. Commun. **20**, 611 (1965)
60. G.L. Eichhorn, P. Clark, Proc. Nat. Acad. Sci. U.S.A. **53**, 586 (1965)
61. H. Venner, C. Zimmer, Biopolymers **4**, 321 (1966)
62. G.L. Eichhorn, Y.A. Shin, J. Am. Chem. Soc. **90**, 7323 (1968)
63. H.K.S. Souza, Thermochim. Acta **501**, 1 (2010)
64. H. Yang, K.L. Metera, H.F. Sleiman, Coord. Chem. Rev. **254**, 2403 (2010)
65. J.S. Lee, L.J.P. Latimer, R.S. Reid, Biochem. Cell Biol. **71**, 162 (1993)
66. P. Aich, S.L. Abiuk, L.W. Tari, L.J.T. Delbaere, W.J. Roesler, K.J. Falk, R.P. Steer, J.S. Lee, J. Mol. Biol. **294**, 477 (1999)
67. Y. Miyake, H. Togashi, M. Tashiro, H. Yamaguchi, S. Oda, M. Kudo, Y. Tanaka, Y. Kondo, R. Sawa, T. Fujimoto, T. Machinami, A. Ono, J. Am. Chem. Soc. **128**, 2172 (2006)
68. Y. Tanaka, S. Oda, H. Yamaguchi, Y. Kondo, C. Kojima, A. Ono, J. Am. Chem. Soc. **129**, 244 (2007)
69. K. Tanaka, G.H. Clever, Y. Takezawa, Y. Yamada, C. Kaul, M. Shionoya, T. Carell, Nat. Nanotechnol. **1**, 190 (2006)
70. M. Daune, C.A. Dekker, H.K. Schachman, Biopolymers **4**, 51 (1966)
71. A. Ono, S. Cao, H. Togashi, M. Tashiro, T. Fujimoto, T. Machinami, S. Oda, Y. Miyake, I. Okamoto, Y. Tanaka, Chem. Commun. 4825 (2008)
72. S.V. Kornilova, L.E. Kapinos, A. Tomkova, P. Mishkovskii, Y.P. Blagoi, T.V. Bol'bukh, Biophysics **39**, 407 (1994)
73. V.V. Andrushchenko, S.V. Kornilova, L.E. Kapinos, E.V. Hackl, D.N. Grigoriev, V.L. Galkin, Y.P. Blagoi, J. Mol. Struct. **408**, 225 (1997)
74. L. Yang, T.A. Keiderling, Biopolymers **33**, 315 (1993)
75. D.O. Wood, J.S. Lee, J. Inorg. Biochem. **99**, 566 (2005)
76. J. Duguid, V.A. Bloomfield, J. Benevides, J.G. Jr, Thomas. Biophys. J. **69**, 2623 (1995)
77. A.M. Polyanichko, V.V. Andrushchenko, E.V. Chikhirzhina, V.I. Vorob'ev, H. Wieser, Nucl. Acids Res. **32**, 989 (2004)

78. V.A. Bloomfield, Biopolymers **31**, 1471 (1991)
79. V.A. Bloomfield, Biopolymers **44**, 269 (1998)
80. S. Ghosh, E. Defrancq, Chem. Eur. J. **16**, 12780 (2010)
81. H. Yang, H.F. Sleiman, Angew. Chem. Int. Ed. **47**, 2443 (2008)
82. H. Yang, C.K. McLauglin, F.A. Aldaye, G.D. Hamblin, A.Z. Rys, I. Rouiller, H.F. Sleiman, Nat. Chem. **1**, 390 (2009)
83. K. Tanaka, A. Tengeiji, T. Kato, N. Toyama, M. Shionoya, Science **299**, 1212 (2003)
84. G.H. Clever, T. Carell, Angew. Chem. Int. Ed. **46**, 250 (2007)
85. S. Johannsen, N. Megger, D. Böhme, R.K.O. Sigel, J. Müller, Nature Chem. **2**, 229 (2010)
86. A.M. Pizarro, P.J. Sadler, *Metal Ion-Nucleic Acid Interactions in Disease and Medicine*, in Nucleic Acid-Metal Ion Interactions, ed. by N.V. Hud (RSC Publishing, Cambridge, 2009)
87. E.R. Jamieson, S.J. Lippard, Chem. Rev. **99**, 2467 (1999)
88. H. Köpf, P. Köpf-Maier, Angew. Chem. **91**, 509 (1979)
89. C.G. Hartinger, S. Zorbas-Seifried, M.A. Jakupec, B. Kynast, H. Zorbas, B.K. Keppler, J. Inorg. Biochem. **100**, 891 (2006)
90. G. Sava, A. Bergamo, S. Zorzet, B. Gava, C. Casarsa, M. Cocchietto, A. Furlani, V. Scarcia, B. Serli, E. Iengo, E. Alessio, G. Mestroni, Eur. J. Cancer **38**, 427 (2002)
91. J.J. Gooding, Analyst **132**, 603 (2007)
92. H. Torigoe, A. Ono, T. Kozasa, Transition Met. Chem. **36**, 131 (2011)
93. Z. Lin, X. Li, H.-B. Kraatz, Anal. Chem. **83**, 6896 (2011)
94. X. Bin, H.-B. Kraatz, Analyst **134**, 1309 (2009)
95. Y.T. Long, C.Z. Li, H.-B. Kraatz, J.S. Lee, Biophys. J. **84**, 3218 (2003)
96. X. Li, J.S. Lee, H.-B. Kraatz, Anal. Chem. **78**, 6096 (2006)
97. X. Li, Y. Zhou, T.C. Sutherland, B. Baker, J.S. Lee, H.-B. Kraatz, Anal. Chem. **77**, 5766 (2005)
98. M.H. Shamsi, H.-B. Kraatz, Analyst **135**, 2280 (2010)
99. P.M. Diakowski, H.-B Kraatz, Chem. Commun. 1189 (2009)
100. B. Liu, A.J. Bard, C.Z. Li, H.-B. Kraatz, J. Phys. Chem. B **109**, 5193 (2005)
101. M.H. Shamsi, H.-B. Kraatz, Analyst **136**, 4724 (2011)
102. P.M. Diakowski, H.-B. Kraatz, Chem. Commun. 1431 (2011)
103. J.B. MacNaughton, A. Moewes, J.S. Lee, S.D. Wettig, H.-B. Kraatz, L.Z. Ouyang, W.Y. Ching, E.Z. Kurmaev, J. Phys. Chem B **110**, 15742 (2006)
104. A. Rakitin, P. Aich, C. Papadopoulos, Y. Kobzar, A.S. Vedeneev, J.S. Lee, J.M. Xu, Phys. Rev. Lett. **86**, 3670 (2001)
105. C. Adessi, M.P. Anantram, J. Mol. Model. **82**, 2353 (2003)
106. Y.V. Rubin, L.F. Belous, A.A. Yakuba, J. Mol. Model. **17**, 997 (2011)
107. G. Brancolini, R.D. Felice, J. Chem. Phys. **134**, 205102 (2011)
108. R. Dong, X. Yan, K. Li, G. Ban, M. Wang, S. Cui, B. Yang, Nanoscale Res. Lett. **5**, 1431 (2010)